Petroleum Science 22 (2025) 3967–3990

Contents lists available at ScienceDirect

Petroleum Science

journal homepage: www.keaipublishing.com/en/journals/petroleum-science

Review Paper

# Thermal maturity effect on the microscopic pore structure and gas adsorption capacity of shale gas reservoirs: A review

Wei-Dong Xie [a,b,*], Xiao-Fei Fu [a,**], Hai-Xue Wang [a], Yu Sun [a], Veerle Vandeginste [c], Xiao-Peng Li [d]

[a] School of Earth Sciences, Northeast Petroleum University, Daqing, 163318, Heilongjiang, China
[b] State Key Laboratory of Continental Shale Oil, Northeast Petroleum University, Daqing, 163318, Heilongjiang, China
[c] KU Leuven, Campus Bruges, Department of Materials Engineering, Bruges BE, 8200, Belgium
[d] School of Earth Sciences and Spatial Information Engineering, Hunan University of Science and Technology, Xiangtan, 411201, Hunan, China

ARTICLE INFO

*Article history:*
Received 1 August 2024
Received in revised form
10 June 2025
Accepted 29 July 2025
Available online 6 August 2025

Edited by Jie Hao and Xi Zhang

*Keywords:*
Shale gas reservoirs
Thermal maturity
Organic matter pores
Adsorption capacity
Hydrocarbon generation

ABSTRACT

Organic matter (OM) is the primary gas occurrence carrier in shale reservoirs due to their abundant nanopores. To reveal the OM pore structure, adsorption capacity and evolution during thermal maturation, this study collected data from samples spanning the entire evolution stage, from immature to over-mature. Scanning Electron Microscope (SEM) observation and low temperature gases adsorption experiments were used to qualitatively-semi-quantitatively and quantitatively analyze OM pore structure evolution, and $CH_4$ isothermal adsorption experiments were used to reveal the adsorption capacity evolution. Then, the influence and mechanism of maturity and hydrocarbon generation on pore development and adsorption capacity were quantitatively reviewed based on the experimental data. The results show that OM pores are poorly developed in the immature stage due to weak hydrocarbon generation, although micro-fractures are occasionally found at the edges of OM particles. In the low maturity stage, OM pores are partially developed due to liquid hydrocarbon generation, with liquid hydrocarbons also filling some OM pores. The contribution of total organic carbon content (TOC) to adsorption extent is not significant in these two stages. From high to high-over maturity stages, massive gaseous hydrocarbons are generated, significantly improving the surface porosity of OM. Clear positive linear correlations are observed between TOC and adsorption amount. However, the development of OM pores significantly declines when thermal maturity ($R_o$) exceeds 3.5% due to excessive aromatization. The accuracy of research on the evolution of pore structure and adsorption capacity is limited by several factors: (i) errors caused by sample specification, calculation processes, parameter settings, and kerogen models in isothermal adsorption experiments and molecular simulations; (ii) difficulty in achieving control variables due to the strong heterogeneity of natural maturation shale samples; and (iii) the need to enhance compatibility between thermal simulation experiments and natural thermal evolution. Therefore, isothermal adsorption experiments on bulk shale and molecular simulations of intact shale model are necessary, taking into account the dynamic temperature and pressure of in-situ reservoirs. Moreover, shale samples with varying maturity, influenced by their distance from the paleo-thermal source, may provide significant verification for thermal simulation experiments.


## 1. Introduction

Several countries have successfully achieved large-scale commercial exploitation of shale gas, significantly alleviating the excessive consumption of conventional energy (Salygin et al., 2019; Bakshi and Vishal, 2021; Luo et al., 2025). Shale gas refers to unconventional natural gas stored in organic-rich mudstone/shale, primarily in adsorbed and free states (King, 1993; Curtis,

* Corresponding author.
** Corresponding author.
*E-mail addresses:* xwd@cug.edu.cn (W.-D. Xie), fxf@nepu.edu.cn (X.-F. Fu).
Peer review under the responsibility of China University of Petroleum (Beijing).

https://doi.org/10.1016/j.petsci.2025.07.023

2002). The desorption, migration, and production of adsorbed gas, which accounts for 20%–85% in shale gas reservoirs (Curtis, 2002), are crucial for enhancing gas recovery due to the complex pore structure and adsorption mechanism of shale gas reservoirs (Swami and Settari, 2012; Liu, 2020; Fan et al., 2022). OM is the primary adsorption carriers of shale gas due to its extensively developed nanopores, especially in high maturity and over-maturity shale gas reservoirs with higher exploration potential (Passey et al., 2010; Lis et al., 2025; Lu et al., 2025). Although clay is another important adsorption carrier in shale, its effect on adsorbed gas content is significant only in samples with low TOC or low thermal maturity (Qiao et al., 2020; Xie et al., 2022a). OM pores are mainly formed during hydrocarbon generation, consisting of oval, concave and crescent shaped pores at micron to nano scale, and micro-fractures with micron-scale length and nano-scale width developed at the edge of OM and minerals (Loucks et al., 2012; Loucks and Reed, 2015; Löhr et al., 2015). The development features of pore structure in shale gas reservoirs can be obtained through qualitative and quantitative methods such as visual observation (SEM observation), fluid injection (includes Mercury Injection, Low-temperature $N_2$ and $CO_2$ Adsorption, and Nuclear Magnetic Resonance experiments), and digital reconstruction (construction of 3D models of pore structure based on CT Scanning technique) (Tang et al., 2021; Fleury et al., 2022; Chandra et al., 2025). Experimental results show that micro and nano pores are widely developed in OM, especially nanopores, which are the primary controlling factors of porosity, permeability, pore volume (PV), and specific surface area (SSA) of shale gas reservoirs (Tang et al., 2015a; He et al., 2020). Furthermore, gas accumulation, migration, and occurrence features are controlled by TOC to some extent, determined by the development of OM pore type, pore size, and their connectivity (Romero-Sarmiento et al., 2013; Furmann et al., 2014; Awan et al., 2024).

TOC affects adsorption capacity by providing substantial PV and SSA as the adsorption site and storage space for shale gas. It is a significant parameter for strategic selection and resource evaluation of shale gas reservoirs (Ross and Bustin, 2009; Rojas et al., 2024). Yuan et al. (2019) suggested that PV and SSA of micropores (pores with diameter <2 nm according to Rouquerol et al. (1994)) in shale are predominantly contributed by TOC. Additionally, the development of mesopores (pores with diameter in the range of 2–50 nm according to Rouquerol et al. (1994)) in shale is also controlled by TOC, with clear positive linear correlations recorded between TOC and PV and SSA (Guo et al., 2019). In contrast, the contribution of TOC to the development of macropores in shale is variable; even samples collected from the same formation in the same basin may show different correlations (Sun et al., 2016, 2020a). Liang et al. (2015) indicated that TOC also significantly impacts the roughness of pore surfaces, besides PV and SSA. The influence of TOC on the adsorption capacity of shale exhibits various correlations (Gasparik et al., 2012; Zhong et al., 2016). Wang et al. (2019a) and Xie et al. (2021a) demonstrated that the impact of TOC on the adsorption amount of shale is much higher than other adsorption carriers, resulting in no obvious correlation or even a negative correlation of mineral composition versus adsorption amount. Bu et al. (2015) and Chen et al. (2020a) implied that clay minerals contribute more to the adsorption amount than TOC. The reason behind this phenomenon is that the contribution of OM to the adsorption capacity of shale does not only depend on its content, but also on its thermal maturity (Curtis et al., 2012; Zhao et al., 2018; Hazra et al., 2020). Wang et al. (2019b) and Cao et al. (2021) demonstrated that the development of OM pores and adsorption capacity of shale is controlled by hydrocarbon generation, with the development of nanopores often corresponding to the peak of hydrocarbon generation. Consequently, the role of OM in pore development and adsorption capacity of shale gas reservoirs during thermal evolution needs to be clarified.

Xie et al. (2021b) discussed the pore development features of shale samples of low maturity, high maturity, and over-maturity, respectively, and demonstrated that more OM pores are developed with higher thermal maturity. Zhang et al. (2020a) also proved that the contribution of OM pores to porosity and connectivity in higher maturity samples is greater than in lower maturity shale samples. The coupled control of TOC and thermal maturity on OM pores is also confirmed by thermal simulation experiments (Hu et al., 2015; Xu et al., 2021a). Nevertheless, Miao et al. (2017) and Tenger et al. (2021) revealed that the promotion of thermal maturity to OM pores is not endless; the pore structure is destroyed when reaching a certain value. Although researchers have conducted significant scientific research on the pores and adsorption characteristics of shale, several crucial issues still need more systematic work: (i) Natural maturation samples and thermal simulation experiments are mostly staged, ignoring the continuity of the thermal evolution process. (ii) There is a lack of research and review on the evolution of pores and adsorption capacity of OM perfectly covering immature to high-over maturity (refers to $R_o > 2.5\%$ in this study) stages. (iii) Quantitative research regarding the pore development in organic debris in shale is rare. (iv) Mutual verification of OM pore development in continuous natural maturation samples and thermal simulation experiments is lacking. Additionally, (v) a comprehensive pattern on the development characteristics and control mechanism of OM pores during diagenetic evolution is rare. Therefore, this review systematically summarizes and assesses the relevant scientific literature on the research of OM pores and adsorption capacity of shale. The thermal evolution stages of source rocks are divided based on $R_o$ of OM. The isothermal adsorption experimental results of shale samples from immature to high-over maturity are collected, and the evolution of the contribution of TOC to the adsorption amount is discussed correspondingly. Quantitative characterization of OM pores evolution by the surface porosity of OM in SEM images is performed, and the natural maturation shale samples and thermal simulation experimental results are mutually verified. Subsequently, a comprehensive evolution pattern of OM pores and adsorption capacity of shale is established based on the results of thermal evolution, diagenetic processes, and hydrocarbon generation evolution. Moreover, the current challenges in this field are condensed, and further research direction and potential schemes are pertinently proposed. Results from this review reveal the controlling mechanism (hydrocarbon generation type, amount, peak, reaction mechanism of OM, etc.) of OM pores evolution, which are of specific theoretical significance for the design of exploitation schemes of shale gas reservoirs with different thermal maturity.

## 2. Development features of OM and internal pores in shale gas reservoirs

### 2.1. Development of OM in global industrial shale gas reservoirs

OM is the source of oil and natural gas in shale gas reservoirs. Hydrocarbons are generated through the cracking of OM as thermal evolution proceeds, successively reaching the peak of oil and gas generation (Fookes et al., 1990; Hunt, 1991). Additionally, OM pores are the primary components of the pore system in shale gas reservoirs. These pores can from throughout the hydrocarbon generation process, including those created by hydrocarbon generation and expulsion, as well as dissolved pores formed by organic acids (Milliken et al., 2013; Xu et al., 2021b; Xing et al.,

2021). Therefore, TOC is a significant parameter for evaluating and exploiting industrial shale gas reservoirs (Ross and Bustin, 2009; Rojas et al., 2024). Shale gas is more easily enriched in continuous and OM rich reservoirs (Mani et al., 2017; Ghanizadeh et al., 2020). Peters (1986) classified the generative potential of source rock into four grades: poor, fair, good, and very good, with TOC values of 0–0.5, 0.5–1, 1–2, and >2, respectively. Overall, TOC varies dramatically in global industrial shale gas reservoirs (Table 1). North America was the first region to achieve large-scale commercial development of shale gas, including multiple formations in the Appalachia, Fort Worth, and Michigan basins (Harper, 2008; Jiao, 2019). Marcellus, Fayetteville, Barnett, Ohio, and Antrim shales are rich in OM and have undergone thermal maturation and hydrocarbon generation processes, leading to higher gas content in reservoirs. Among them, the Fayetteville and Barnett shales have high and stable TOC, resulting in the best gas content. In comparison, the Lewis shale in the San Juan Basin has relatively low TOC, resulting in the lowest gas content (Table 1). In China, a breakthrough in the Longmaxi shale gas reservoirs has been achieved, including areas such as Changning and Jiaoshiba (Long et al., 2018; Wang, 2019). The average gas content of Longmaxi shale in the Changning area (5.3 $cm^3/g$) is higher than that in the Jiaoshiba area (1.97 $cm^3/g$). This difference in TOC (4.0% and 2.54% on average for them, respectively) (Table 1) may be a significant reason for this phenomenon, although gas content is also affected by burial depth, geological tectonics, mineral composition, seal capacity, etc. Additionally, Wang et al. (2013), Yang et al. (2016a), Guo and Peng (2019), and Liu et al. (2019a) reported that high TOC generally corresponds to large porosity and gas content. The Doushantuo shale of the Sinian, Niutitang shale of the Cambrian, and Dalong shale of the Permian are also expected to achieve commercial exploitation. Their TOC meets the requirements for good to very good shale gas reservoirs (Table 1) according to Peters's classification (Peters, 1986), indicating strong hydrocarbon generation capacity. However, the Niutitang shale in Well EY1 and Well HY1 have the highest TOC in Table 1, with an average of 6.09% and 5.5%, respectively, which is obviously higher than the commercially developed Longmaxi shale. Despite this, their gas content is the lowest (0.26% and 0.89% on average). Therefore, the abundance of OM is not the critical obstacle to their industrial production. Compared to North America, the tectonics of China are more complex, especially in the southern region (Xiao et al., 2015a; Dong et al., 2016). The diagenesis and hydrocarbon generation evolution processes of shale also vary significantly, and tectonic transformation after gas accumulation lead to substantial differences in gas content (Ju et al., 2014; Xiao et al., 2015a; Zhou et al., 2022). Structural location, fault development, burial depth, reservoir thickness, and continuity, are also important indicators for shale gas selection, in addition to TOC (Ma, 2019; Yi et al., 2019). Overall, TOC affects the original hydrocarbon generation capacity of shale gas reservoirs and is a significant factor influencing gas accumulation capacity. Commercial shale gas reservoirs generally have high TOC values.

### 2.2. Typical OM pores in shale gas reservoirs

The pore classification scheme of Loucks et al. (2009) is widely recognized, comprising OM pores, intergranular pores, intragranular pores, and micro-fractures. OM pores are the most developed in industrial shale gas reservoirs and can be further divided into several types based on origin, development location, pore shape, connectivity, and quantity (Fig. 1). Primary pores and secondary pores are distinguished by their origin. Primary pores include biological reticular fiber structures, cell cavities, animal cavities, and intermolecular micro-fractures (Fig. 1(i)–(k)). During the thermal evolution of source rocks, primary OM pores undergo mechanical compaction and filling with liquid OM (mainly liquid bitumen formed during hydrocarbon generation), which gradually deteriorates and even disappears (Löhr et al., 2015; Ghanizadeh et al., 2020; Zhu et al., 2022). Secondary pores include hydrocarbon generation pores, micro-fractures, and mold pores (Fig. 1(a)–(h), (l)–(p)). Hydrocarbon generation pores are mostly developed at micron to nano scale, consisting of bubble-shaped pores (Fig. 1(a)–(c), (e), (g)), honeycomb shaped pores (Fig. 1(d)), and amorphous pores (Fig. 1(f)). Micro-fractures include hydrocarbon generation shrinkage fractures within OM and diagenetic shrinkage micro-fractures at the edge of OM and other minerals (Fig. 1(h)–(l)–(o)). Mold pores are formed by the dissolution of inner

**Table 1**
TOC, porosity, and gas content of the global industrial shale gas reservoirs.

| Commercial shale | Basin/area/well | TOC, % | Porosity, % | Gas content, $cm^3/g$ |
|---|---|---|---|---|
| North America | | | | |
| Marcellus | Appalachian | 3.0–12 | – | 1.7–2.8 |
| Fayetteville | Arkoma | 4–9.8 | 2.0–8.0 | 1.7–6.2 |
| Barnett | Fort Worth | 1.0–13 | 4.0–5.0 | 4.2–9.9 |
| Lewis | San Juan | 0.45–2.5 | – | 0.42–1.28 |
| Ohio | Appalachian | 0.5–23 | 2.0–11 | 1.7–2.83 |
| Antrim | Michigan | 0.3–24 | 2.0–10 | 1.13–3.5 |
| China | | | | |
| Niutitang | Well ZD-2 | 0.41–5.02 (2.61) | 1.95–3.72 (2.67) | 0.78–4.44 (2.27) |
| | Well ZD-1 | 0.53–8.72 (3.14) | 1.18–3.46 (2.26) | 0.18–5.58 (2.24) |
| | Well EY1 | 1.02–11.15 (6.09) | – | 0.11–0.39 (0.26) |
| | Well HY1 | 0.18–11.03 (5.5) | – | 0.23–1.8 (0.89) |
| Longmaxi | Well YD-1 | 0.70–6.29 (2.49) | 0.97–2.16 (1.65) | 0.57–3.31 (1.65) |
| | Well XD-2 | 0.65–8.08(1.95) | 1.17–3.10 (2.36) | 0.63–3.45 (1.56) |
| | Changning | 1.9–7.3 (4.0) | – | 3.1–7.8 (5.3) |
| | Jiaoshiba | 0.55–5.89 (2.54) | – | 0.44–5.19 (1.97) |
| Doushantuo | Well ZD-1 | 0.72–2.91 (1.63) | 1.19–3.41 (2.16) | 0.47–1.50 (0.95) |
| | Well ZD-2 | 0.07–1.78 (0.66) | 1.42–3.93 (2.27) | 0.14–1.67 (0.80) |
| Dalong | ED-1 | 0.11–17.04 (5.91) | 2.64–8.34 (5) | 1.02–2.52 (1.85) |
| | JD-3 | 1.9–9 (5.28) | 0.5–8.36 (1.38) | 1.51 |

Notes: data of shale gas reservoirs in North America refer to Montgomery et al. (2005), Bowker (2007), Jarvie et al. (2007), Carter et al. (2011), Slatt and O'Brien (2011), Shan et al. (2015), Deng et al. (2020), and Shao et al. (2021). Data of shale gas reservoirs in China refer to Zhang et al. (2015a), Zhao et al. (2019); Zou et al. (2021), Xu et al. (2021c), and Tao et al. (2023).

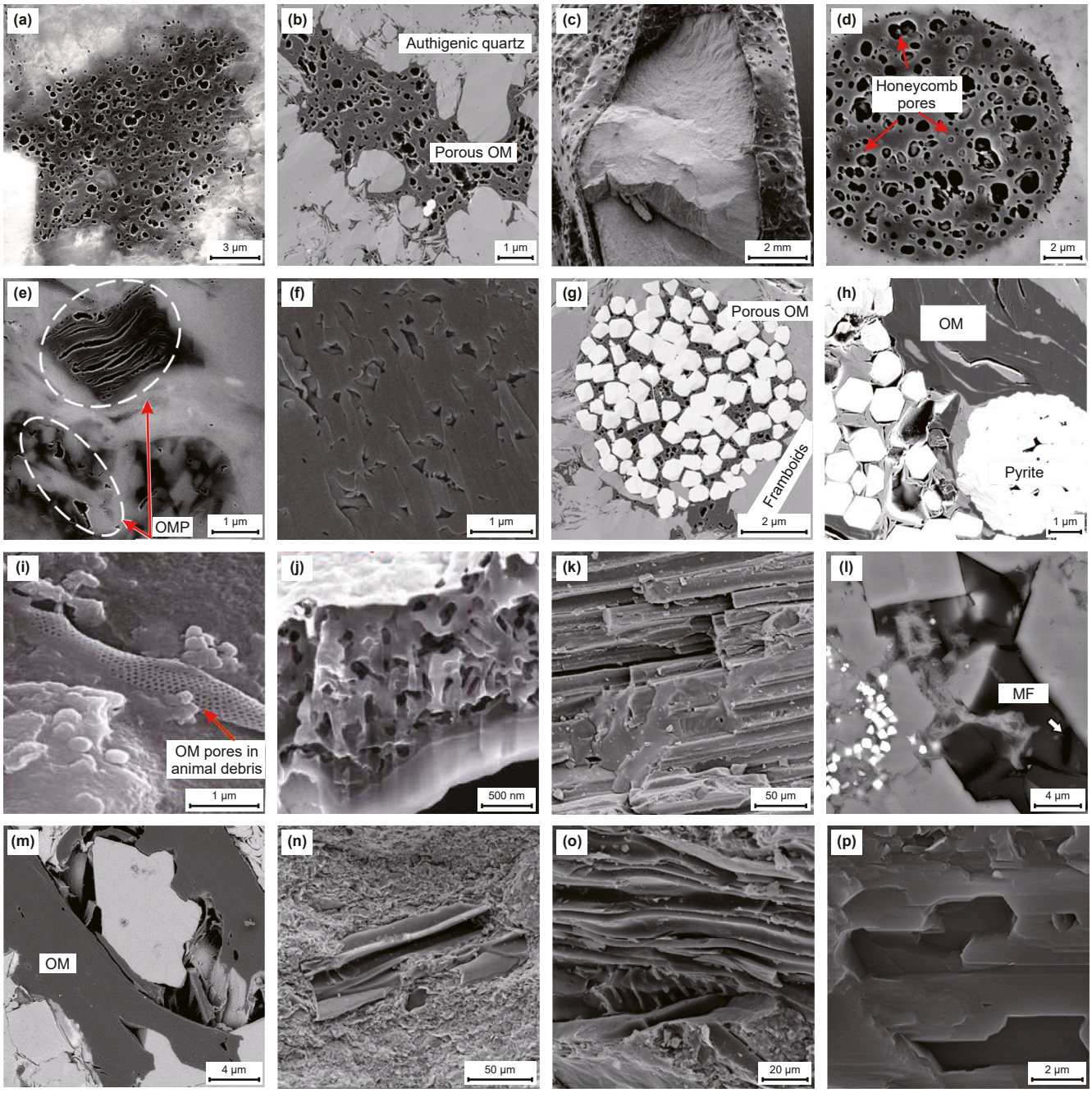


**Fig. 1.** Typical OM pores in shale gas reservoirs. OM is organic matter, OMP is OM pores, MF is micro-fractures. (**a**) (Lower Silurian shale, Sichuan Basin) and (**b**) (Longmaxi shale, Sichuan Basin) reproduced with permission from Li et al. (2020a) and Hu et al. (2020a). OM is filled among brittle minerals, oval - circular bubble OM pores developed at micron to nano scale. (**c**) (Permian shale, Ordos Basin). Thin film OM wraps shale debris, oval - circular bubble OM pores developed at micron scale. (**d**) (Haynesville shale, Louisiana) reproduced with permission from Klaver et al. (2015). Bubble OM pores densely developed in honeycomb shape. (**e**) (Goldwyer shale, Canning Basin) and (**f**) (Da'anzhai shale, Sichuan Basin) reproduced with permission from Gao et al. (2016) and Yuan et al. (2021). Strip shaped and amorphous OM pores developed at micron to nano scale. (**g**) (Lower Silurian shale, Sichuan Basin) and (**h**) (Permian shale, Ordos Basin) reproduced with permission from Li et al. (2020a) and Qiu et al. (2021). Pyrite is filled in OM. (**i**) (Niutitang shale, Zunyi) and (**j**) (Wufeng-Longmaxi shale, Sichuan Basin) reproduced with permission from Tenger et al. (2021). Oval and amorphous OM pores developed in graptolite and other animal debris. (**k**) (Permian shale, Ordos Basin). Micro-fractures (the length is at micron-scale and width is at nano-scale) developed among fusinite splitter and a few oval pores developed. (**l**) (Yanchang shale, Ordos Basin) and (**m**) (Lucaogou shale, Junggar Basin) reproduced with permission from Kuang et al. (2022). Micro-fractures (the length is at micron-scale and width is at nano-scale) developed at the edge of OM. (**n**) and (**o**) (Permian shale, Ordos Basin). Micro-fractures developed among lamellar OM. (**p**) (Permian shale, Ordos Basin). Mold pores developed in OM at micron scale.

minerals, retaining the crystal shape of these minerals (Fig. 1(p)). Different types of OM pores are characterized by distinct morphology and structure (Nie et al., 2019a; Tang et al., 2019). Pores are categorized into tubular pores, ink-shaped pores, plate pores, stacked pores, slit pores, and mold pores based on their morphology (Fig. 2) (Sun et al., 2020a; Wang et al., 2020a; Xie et al., 2022a). Hydrocarbon generation pores are mainly ink-shaped, and can evolve into tubular pores when interconnected (Fig. 1(a)–(d), (g), Fig. 2(a) and (b)). Certain slit pores are also present (Fig. 1(e) and (f), and Fig. 2(e)). The morphology of micro-fractures resembles plate pores and stacked pores (Fig. 1(k)–(o) and Fig. 2(c) and (d)). Mold pores retain the crystal or aggregate

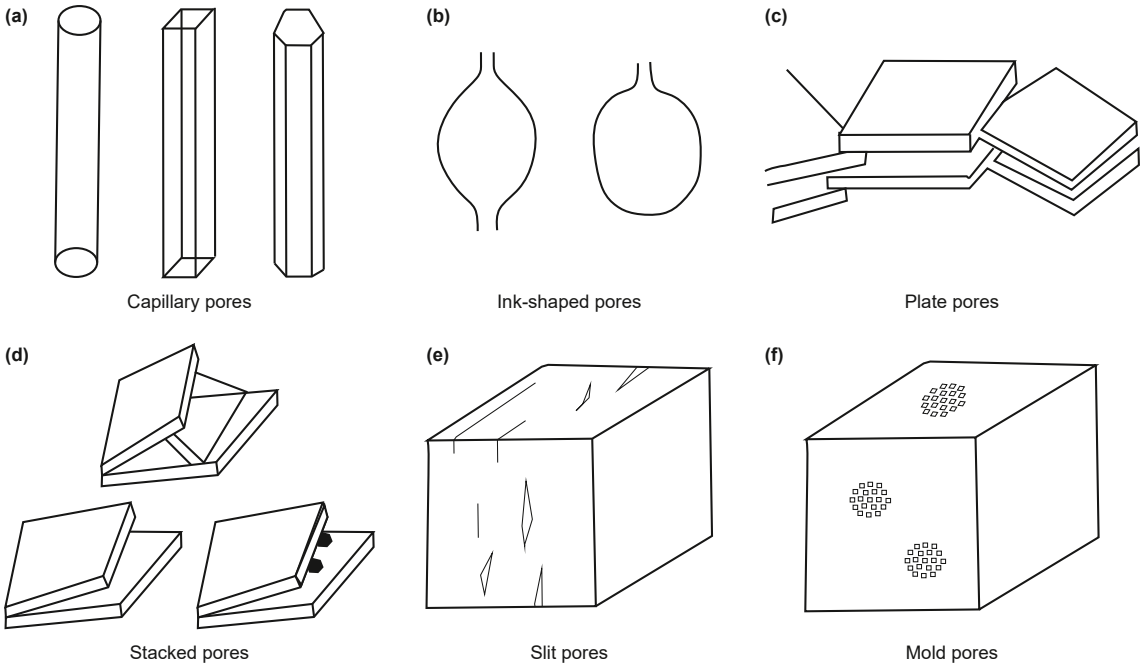


**Fig. 2.** Skeleton model of typical pores in shale gas reservoirs. Reproduced with permission from Xie et al. (2022a).

shape of mold minerals, which may be slightly altered by diagenesis (Figs. 1(p) and 2(f)). Higher TOC usually corresponds to more developed nanopores, influencing pore size distribution and enhancing the connectivity and surface complexity of OM pores (Guo et al., 2015; Yang et al., 2019). Yang et al. (2014, 2016b) indicated that the fractal dimension of shale pores ranges from 2.68 to 2.83, with higher TOC promoting a larger fractal dimension. They stated that TOC improves the development of PV and SSA, especially for micropores, while decreasing pore diameter. Hence, rougher pore surfaces and more complex pore structures are formed, enhancing the adsorption capacity for $CH_4$ (Yang et al., 2014, 2016b).

## 3. Effect of TOC on shale adsorption capacity

Currently, TOC is considered the crucial factor influencing shale adsorption capacity (Kim et al., 2017; Ye et al., 2017; Bakshi and Vishal, 2021). Experimental and molecular simulations are extensively employed to investigate the adsorption behavior and mechanism of $CH_4$ in shale gas reservoirs (Yuan et al., 2014; Psarras et al., 2017). Isothermal adsorption instruments and nuclear magnetic resonance instruments are widely used to analyze shale adsorption capacity (Veselinovic et al., 2018; Aji et al., 2022). Adsorption isotherms of $CH_4$ in both shale and isolated kerogen are classified as type I isotherms by the International Union of Pure and Applied Chemistry. The adsorption amount increases with higher experimental pressure until equilibrium is reached, but the increments gradually decrease during this process (Li et al., 2017; Wang et al., 2019a). The adsorption amount decreases with higher temperature at the same pressure, and thermodynamic parameters such as adsorption heat, entropy, and Gibbs free energy can be calculated from adsorption isotherms at different temperatures (Dang et al., 2017; Xie et al., 2023). $CH_4$ adsorption is a physisorption process with isosteric heat lower than 42 kJ/mol (Rexer et al., 2014; Wu et al., 2015a; Li et al., 2019a). It is a spontaneous, exothermic, and enthalpy-driven process determined by positive Gibbs free energy and negative entropy and enthalpy changes (Rexer et al., 2014; Wu et al., 2015a; Li et al., 2019a; Xie et al., 2023). Additionally, the isosteric heat and adsorption entropy of isolated kerogen are higher than those of whole shale, indicating strong adsorption strength in kerogen (Li et al., 2018). Temperature and pressure critically impact the thermodynamic and kinetic processes of $CH_4$ adsorption, varying greatly with different burial depths or regions due to varying pressure and temperature gradients (Wu et al., 2015a; Xie et al., 2021c). Understanding these influences is crucial for predicting in-situ gas content and promoting $CH_4$ desorption to enhance gas recovery. Temperature inhibits adsorption capacity by increasing thermal motion, molecular kinetic energy, and self-diffusion coefficient, allowing $CH_4$ to overcome van der Waals and electrostatic forces and escape from adsorption sites. This results in decreased isosteric heat, Gibbs free energy, surface potential energy, adsorption rate, and gas residence time on pore surfaces, reducing the spontaneity, affinity, and intensity of adsorption (Dang et al., 2017; Hu et al., 2020b; Hao et al., 2021). Conversely, pressure promotes adsorption capacity, having the opposite effect of temperature.

Researchers generally agree that OM is the most important adsorption carrier of $CH_4$ in shale gas reservoirs, contributing significantly more than clay and brittle minerals (Zhang and Fu, 2018; Wang et al., 2021). Li et al. (2017) conducted high-pressure isothermal adsorption experiments on the Qiongzhusi shale (Lower Cambrian) from eastern Yunnan Province, China, discussing the relationships among $CH_4$ adsorption amount, TOC, and pore structure parameters. Both micropores and mesopores-macropores show positive correlations with TOC, whereas the influence of clay and quartz content on $CH_4$ adsorption is better reflected after normalizing adsorption amounts by TOC (Li et al., 2017; Wang et al., 2019a; Xie et al., 2021a). Yang et al. (2014) proposed that the adsorption capacity of shale gas reservoirs (Lower Cambrian shale, Sichuan Basin, China) is controlled by the SSA of micropores, primarily contributed by OM. Moreover, the fractal dimension of shale is controlled by TOC, leading to higher adsorption amounts and stronger adsorption capacity (Yang et al., 2014). Chen et al. (2015), Sun and Guo (2018), and Bao et al. (2020)

found that mesopores significantly contribute to SSA and adsorption capacity of shale, alongside micropores, whereas macropores play a less obvious role. In contrast, Zhong et al. (2016), Qiao et al. (2020), Liu et al. (2022a), and Xie et al. (2021b) found that clay content contributes more significantly to pore parameter or adsorption capacity than OM, due to their samples having low thermal maturity, low TOC or similar TOC characteristics. This study tests the adsorption capacity of Cretaceous shale gas reservoirs using isothermal adsorption instruments, discussing the contribution of TOC to shale adsorption capacity. A negative linear correlation is observed between TOC and Langmuir volume ($V_L$), with clay minerals being the main contributors to shale adsorption amounts. The negative correlation or lack of clear correlation is attributed to the lower thermal maturity stage and poor development of OM pores in these samples (Fu et al., 2015; Cavelan et al., 2019; Zhang et al., 2020b). Thermal maturity plays a crucial role in the development of OM pores and enhances shale adsorption capacity (Tang et al., 2015b; Hu et al., 2015; Xu et al., 2021a). Therefore, it is necessary to clarify the evolution of OM pores and adsorption capacity in shale gas reservoirs during thermal evolution.

Experimental simulation of $CH_4$ adsorption have greatly advanced the understanding of $CH_4$ adsorption behavior in shale gas reservoirs. However, several drawbacks affect the accuracy and precision of these simulation results: (i) the crushing or grinding process of samples can damage the pore-structure system of the reservoir to some extent. It remains controversial whether powder samples (mostly at 80–100 mesh) accurately represent continuous shale gas reservoirs. (ii) The small sample size required for experiments (mostly less than 10 g) makes it difficult to ensure the accuracy of adsorption calculations, including sample volume/mass, blank tests, buoyancy tests, and free volume tests. (iii) The evolution of temperature and pressure in real shale gas reservoirs is dynamic. However, experiments typically set a fixed temperature and gradually increase pressure, ignoring their coupled effects. (iv) Diverse methods for correcting excess adsorption to absolute adsorption, such as bulk density calculations (using NIST database and Setzmann-Wagner formula (Setzmann and Wagner, 1991; Chen et al., 2020b)) and adsorption phase density calculations (using intercept method or boiling point density (Sircar, 1999; Rexer et al., 2013; Zhou et al., 2016; Gao et al., 2018) lead to varying results. An authoritative scheme is needed. To address these issues, it is necessary to explore effective diffusion methods for $CH_4$ into bulk shale, and develop dynamic models of temperature and pressure in isothermal adsorption instruments. These models should automatically adjust to in-situ conditions based on temperature gradients, pressure gradients, and other reservoir parameters. Neutron Scattering Spectrometer is a potential technique for accurately calculating adsorption phase density and bulk density, although its application is limited by the difficulty of adjusting neutron flux.

## 4. Thermal evolution and its influence on the adsorption capacity of shale gas reservoirs

Clay is another significant adsorption carrier of $CH_4$ in shale gas reservoirs besides OM (Glorioso and Rattia, 2012; Dastidar et al., 2025), with its content ranging from 12% to 78.9% in global commercial shale gas reservoirs (Xie et al., 2022a). Clay minerals contribute significantly to pore structure and adsorption capacity, although their proportion decreasing with further diagenetic evolution (Wu et al., 2015b; Dowey and Taylor, 2020). The type, crystal structure, and pore structure of clay minerals are altered by mechanical compaction chemical compaction. Porosity and connectivity may also be affected by cementation, dissolution and recrystallization (Xie et al., 2021b; Jin et al., 2021). Additionally, OM and clay minerals in shale are often closely combined, sometimes a mosaic pattern, leading to pore blocking and filling in both OM and clay mineral pores, resulting in a more complex pore system (Rexer et al., 2013, 2014; Luo et al., 2019). The evolution of OM and the transformation of clay minerals interact, exhibiting catalytic or inhibitory effects on the evolutionary process through the discharge of interlayer water and cations (Xie et al., 2021a, 2022a). Moreover, geological conditions such as burial depth, pressure, and temperature gradients in different sampling areas significantly influence pore structure and adsorption capacity (Wu et al., 2015b; Boruah et al., 2019; Xie et al., 2021c; Chandra et al., 2023). Therefore, it is necessary to eliminate the influence of these factors when discussing the contribution of OM to pore structure and adsorption capacity in shale gas reservoirs. To achieve this, shale samples at the same maturity stage are mostly collected from the same formation, basin, and study area, and located in the same borehole or profile as much as possible. The sedimentary background and diagenetic evolution process of shale are consistent, and the composition, crystal structure, and pore structure of clay minerals are similar. Nevertheless, there is variability in the clay content of different samples. In the pyrolysis experiments (Section 4.2.2), the same sample was used to discuss the influence of thermal evolution on the pore structure of OM, effectively avoiding the influence of differences in clay minerals.

### 4.1. Relationship between $V_L$ and TOC at different thermal maturity

Undoubtedly, OM pores are crucial for the accumulation of shale gas, and their development is controlled by thermal maturity (Misch et al., 2016; Sun et al., 2019a). As mentioned above, OM affects the pore structure and gas storage capacity of shale through thermal evolution and hydrocarbon generation. OM pores provide significant PV and SSA, and the contribution of TOC to $CH_4$ adsorption varies across shale samples at different thermal evolution stages (Ross and Bustin, 2009; Bakshi et al., 2018; Boruah et al., 2019). Adsorption experiments on 48 shale samples with $R_o$ ranging from 0.46% to 4.25% (from immature to high-over maturity stage) were conducted to explore the changes in TOC contribution to adsorption at different thermal maturity stages (Table 1). The classification of thermal evolution stages follows Tissot et al. (1987): immature stage ($R_o$ < 0.5%), low maturity stage ($R_o$ = 0.5%–1.3%), high maturity stage ($R_o$ = 1.3%–2.0%), over maturity stage ($R_o$ = 2.0%–2.5%), high-over maturity stage (includes two stages of $R_o$ = 2.5%–3.5% and >3.5%). The $V_L$ represents the theoretical adsorption capacity of shale.

In immature shale samples, $V_L$ ranges from 0.32 to 0.41 $cm^3/g$ (0.35 $cm^3/g$ average) with TOC ranging from 1.61% to 5.26% (3.26% average) (Table 2). No significant correlation is observed between $V_L$ and TOC, with data being disorderly distributed ($R^2$ = 0.088) (Fig. 3). OM pores are poorly developed at this stage, and the pore structure is dominated by intergranular primary pores of inorganic minerals, especially clay minerals (Liu et al., 2017a; Zhang et al., 2018a). Mechanical compaction has a greater influence on pores than the thermal evolution of OM (Zhao et al., 2017; Wang et al., 2020b; Xie et al., 2022a). In low maturity shale samples, $V_L$ ranges from 0.829 to 1.081 $cm^3/g$ (0.952 $cm^3/g$ average) with TOC ranging from 0.5% to 1.58% (1.0 % average) (Table 2). A weak negative linear correlation is observed between $V_L$ and TOC ($R^2$ = 0.088) (Fig. 3). At this stage, a large number of liquid hydrocarbons are generated, and OM pores gradually form. However, the presence of crude oil and the filling of liquid OM may occupy OM pores (Loucks et al., 2012; Ma et al., 2017a; Nie et al., 2021). Overall, shale was consolidated affected by mechanical compaction with particles being linear - concave-convex contact, resulting

**Table 2**
Control of TOC on shale adsorption capacity at different thermal evolution stages.

| Immature shale, data from Mishra et al. (2021) | | | Low maturity shale | | | High maturity shale, data from Liu et al. (2013a) | | | Over maturity shale, data from Chen et al. (2019) | | | High-over maturity shale, data from Sun et al. (2015), and Ma et al. (2015) | | | | | |
|---|---|---|---|---|---|---|---|---|---|---|---|---|---|---|---|---|---|
| $R_o$ < 0.5% | | | $R_o$ = 0.5%–1.3% | | | $R_o$ = 1.3%–2.0% | | | $R_o$ = 2.0%–2.5% | | | $R_o$ = 2.5%–3.5% | | | $R_o$>3.5% | | |
| Sample ID | TOC, % | $V_L$, cm$^3$/g | Sample ID | TOC, % | $V_L$, cm$^3$/g | Sample ID | TOC, % | $V_L$, cm$^3$/g | Sample ID | TOC, % | $V_L$, cm$^3$/g | Sample ID | TOC, % | $V_L$, cm$^3$/g | Sample ID | TOC, % | $V_L$, cm$^3$/g |
| CG1302 | 3.52 | 0.34 | DS-1 | 0.66 | 0.956 | L-7 | 2.37 | 2.46 | ND-1 | 0.75 | 1.36 | S-18 | 3.76 | 3.34 | C1-17 | 4.7 | 1.7 |
| CG1306 | 4.24 | 0.34 | DS-2 | 0.5 | 1.058 | L-12 | 7.28 | 3.96 | ND-2 | 2.04 | 1.95 | S-65 | 3.66 | 2.43 | C1-20 | 2.7 | 1.19 |
| CG1312 | 3.96 | 0.32 | DS-3 | 0.5 | 0.956 | L-13 | 10.05 | 4.82 | ND-3 | 2.52 | 2.47 | S-20 | 6.23 | 4.36 | C1-22 | 4 | 1.23 |
| CG1313 | 1.85 | 0.32 | DS-4 | 1.58 | 0.829 | L-15 | 1.77 | 2.03 | ND-4 | 1.63 | 1.45 | S-41 | 9.83 | 5.04 | C1-23 | 4.5 | 1.41 |
| CG1314 | 1.74 | 0.34 | DS-5 | 1.24 | 0.829 | L-16 | 0.79 | 1.96 | ND-5 | 0.813 | 1.34 | S-38 | 1.15 | 2.01 | C1-31 | 2.4 | 1.27 |
| CG1315 | 5.26 | 0.38 | DS-6 | 1.53 | 1.081 | L-17 | 1.07 | 2.4 | ND-6 | 0.427 | 1.05 | S-36 | 0.36 | 1.83 | C1-33 | 3 | 1.2 |
| CG1319 | 3.89 | 0.41 | | | | L-19 | 0.91 | 1.58 | ND-7 | 2.91 | 2.63 | S-66 | 2.81 | 2.62 | C1-36 | 2.3 | 1.1 |
| CG1321 | 1.61 | 0.37 | | | | L-21 | 4.15 | 3.16 | ND-8 | 4.16 | 3.16 | S-60 | 9.74 | 5.23 | | | |
| | | | | | | | | | ND-9 | 1.89 | 1.84 | S-26 | 1.19 | 1.99 | | | |
| | | | | | | | | | ND-10 | 2.38 | 2.34 | | | | | | |

Note: because less research on the adsorption capacity of immature shale was published, $R_o$ of partial immature shale samples ranges from 0.5% to 0.55%.

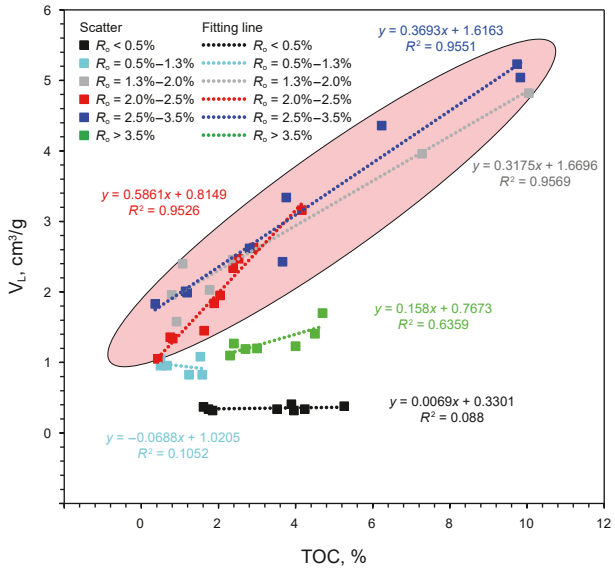


**Fig. 3.** The correlation of TOC and $V_L$ in shale gas reservoirs at different thermal evolution stages. OM is immature ($R_o$ < 0.5%), low mature ($R_o$ = 0.5%–1.3%), high mature ($R_o$ = 1.3%–2.0%), over mature ($R_o$ = 2.0%–2.5%), and high-over mature ($R_o$ = 2.5%–3.5% and >3.5%, respectively), respectively. Data to generate this figure were collected from Mishra et al. (2021), Liu et al. (2013a), Chen et al. (2019), Sun et al. (2015), and Ma et al. (2015).

in serious reduction of primary porosity (Li et al., 2019b; Lu et al., 2022). Besides, the interlayer pores of clay minerals were further reduced with the transformation from smectite to illite and discharge of interlayer water (Zhu et al., 2018a; Wang and Guo, 2020; Ma and Guo, 2021). The iron released in this process formed carbonate and silicate cements, leading to the formation of secondary enlarged edge of quartz, which plays a negative role in porosity (Dowey and Taylor, 2020). Nevertheless, the contribution of inorganic mineral pores is still greater than OM pores at this stage. In high maturity shale samples, the adsorption capacity increases significantly (Table 2). $V_L$ ranges from 1.58 to 4.82 cm$^3$/g (2.80 cm$^3$/g average) with TOC ranging from 0.79% to 10.05% (3.55% average). A clear positive linear correlation is observed between $V_L$ and TOC ($R^2$ = 0.9569) (Fig. 3). At this stage, a large number of gaseous hydrocarbons are generated, and OM pores are well developed (Yin et al., 2017; Song et al., 2020). Due to the impact of mechanical and chemical compaction, inorganic mineral porosity was further decreased, and OM pores began to dominate (Nie et al., 2019b; Liu et al., 2020). Additionally, organic acids produced in hydrocarbon generation process dissolved inorganic minerals and cements in mineral pores, forming some secondary dissolution pores. In over maturity shale samples, dry gas is generated, and OM pores are further developed (Chen et al., 2017; Wei et al., 2019; Li et al., 2019c). $V_L$ ranges from 1.05 to 3.16 cm$^3$/g (1.96 cm$^3$/g average) with TOC ranging from 0.43% to 4.16% (1.95% average). A clear positive linear correlation is observed between $V_L$ and TOC ($R^2$ = 0.9526) (Fig. 3). In the high-over maturity stage ($R_o$ = 2.5%–3.5%), the peak of dry gas generation is reached, and OM pores are extremely well developed (Liu et al., 2019b, 2022b; Xi et al., 2022). The adsorption capacity of shale further increases, and $V_L$ rises linearly with higher TOC ($R^2$ = 0.9551) (Fig. 3). Illitization of smectite proceeded with removal of the last structural water and the continuous mechanical compaction, resulting in the pore size and porosity of minerals were further reduced (Higgs et al., 2007; Shalaby et al., 2014). However, the occurrence of pyrite, quartz, and carbonate supports and protects the intergranular and intragranular pores of clay minerals to some extent through

resisting mechanical compaction (Lai et al., 2015; Wei et al., 2020). Diagenesis of cementation, dissolution, metasomatism, and recrystallization occur widely in the thermal evolution process of shale gas reservoirs. Among them, recrystallization consists mainly of the secondary enlargement of clastic quartz and the transformation of amorphous siliceous minerals to authigenic quartz, both of them are negative to pore development (Heald, 1950; He et al., 2017). Dissolution is constructive to the formation of secondary pores, which mainly occurs in carbonate minerals or potassium feldspar, whereas the organic acid has also a certain impact on clay minerals (Baruch et al., 2015; Elkady and Kovscek, 2020). The influence of metasomatism on pore structure is complex due to the dissolution of original minerals and the formation of new minerals. When thermal maturity further increases ($R_o$ >3.5%), gas generation stops, molecular orientation of OM increases, adsorption heat decreases, and pore development worsens (Wang et al., 2016; Luo et al., 2017; Li et al., 2020b). Nevertheless, TOC still maintains a positive correlation with $V_L$ ($R^2 = 0.6359$), although the adsorption capacity and goodness of fit decrease dramatically (Table 2 and Fig. 3). Additionally, a prominent positive linear correlation is observed between TOC and $V_L$ for $R_o$ values from 1.3% to 3.5% (the pink oval area in Fig. 3), despite samples being collected from different basins with significant component and structure heterogeneity. This confirms the critical contribution of continuous hydrocarbon generation from high maturity to high-over maturity stages to shale pore structure and adsorption capacity.

Several factors affect the influence of TOC on shale adsorption capacity: (i) Although the selected shale samples are in the same thermal evolution stage, $R_o$ clearly varies among samples. (ii) The contribution of OM to adsorption capacity is based on intact shale, ignoring the effects of mineral composition. (iii) The sedimentary background and evolution process of the selected samples differ, resulting in various formation and preservation processes of OM pores, including the sealing capacity of roof and floor strata, the support of rigid minerals and fluid pressure on mechanical compaction. (iv) The macerals of shale samples with different sedimentary backgrounds are distinct, leading to different hydrocarbon generation and pore-forming abilities. Instead of selecting shale samples from different basins, the thermal maturity of shale within the same formation of the same sedimentary basin may show a gradation due to differences in tectonic subsidence or proximity to magmatic intrusion areas. This approach allows for a better discussion of TOC's contribution to shale adsorption capacity while avoiding the influence of the aforementioned factors.

### 4.2. Evolution of the pore structure of OM during the thermal maturation process

#### 4.2.1. Evolution of the pore structure of OM in natural maturation series

During OM maturation, OM pores are formed alongside hydrocarbon generation, which alters the adsorption capacity of shale gas reservoirs by providing accumulation space and adsorption sites for $CH_4$ (Curtis et al., 2013; Löhr et al., 2015). A total of 24 SEM images of shale samples, ranging from immature to high-over mature were collected (Fig. 4). Image J software was utilized to extract the surface porosity (the ratio of the area of OM pores to the area of OM in SEM images) for each image (Fig. 5 and Table 3). Subsequently, the evolution of pore type, pore morphology, pore size, and surface porosity in shale gas reservoirs was quantitively discussed. In immature shale samples (Fig. 4(a)–(d), 5(a)–(d)), gas generation pores are poorly developed. A certain amount of micro-fractures (mostly diagenetic fractures independent of hydrocarbon generation, with micron-scale length and nano-scale width) developed within OM and at the edges of OM and other minerals (Fig. 4(a)–(d), 5(a)–(d)). Some dissolved pores (mainly nano-scale) developed within OM (Fig. 4(c) and 5(c)). These pores are formed by the shrinkage and dissolution associated with diagenesis and OM evolution (Zhang et al., 2019, 2021). The surface porosity ranges from 0 to 2.62%, with an average of 0.86% (Table 3 and Fig. 6(a)). In low maturity shale samples, significant amounts of liquid hydrocarbons are generated, leading to the development of certain hydrocarbon generation pores (mostly elliptical and amorphous beaded isolated pores with poor connectivity at micron to nano scale) and microfractures (Fig. 4(e)–(h), 5(e)–(h)). However, not all OM develops hydrocarbon generation pores, and some pores are difficult to recognize due to the filling of liquid OM (Loucks et al., 2012; Ma et al., 2017b; Nie et al., 2021). The surface porosity gradually increases, ranging from 1.04% to 4.51% (2.86% average) (Table 3 and Fig. 6(a)). In high maturity shale samples, gaseous hydrocarbons (wet gas and condensate gas) are generated, and hydrocarbon generation pores at micro to nano scale are well developed (Fig. 4(i)–(l), 5(i)–(l)). Additionally, isolated OM pores begin to connect (stronger hydrocarbon generation causes the pores to start connecting with each other, still dominated by elliptical and amorphous pores) at this stage (Fig. 4(j)–(l), 5(j)–(l)), which is significant for the accumulation and migration of shale gas (Liu et al., 2018; Song et al., 2020). Surface porosity further increases, ranging from 3.25% to 6.19% (4.72% average) (Table 3 and Fig. 6(a)). In over maturity shale samples, massive dry gas is generated, and the connected OM pores at micro to nano scale are well developed (Fig. 4(m)–(p), 5(m)–(p)). The connectivity of shale pore system is greatly improved at this stage (He et al., 2017; Chen et al., 2017), consisting of the interconnection of elliptical beaded forms elongated pores, the continuous expansion of elliptical pores, and the wide development of small pores embedded within large pore. The surface porosity is dramatically increased, ranging from 9.15% to 29.59% (19.01 average) (Table 3 and Fig. 6(a)). As OM evolves to high-over maturity ($R_o$ = 2.5%–3.5%), the peak of dry gas generation is reached (Stevens et al., 2013; Jin et al., 2018). More hydrocarbon generation pores (mainly nano-scale) develop with particularly good connectivity, further enhancing the three pore connectivity patterns mentioned above (Fig. 4(q)–(t), 5(q)–(t)). Surface porosity reaches its maximum, ranging from 16.17% to 43.19% (average 28.52%) (Table 3 and Fig. 6(a)). However, when OM maturity further increases ($R_o$ > 3.5%), hydrocarbon generation ends, and excessive aromatization destroys the original OM pores (Zhao et al., 2016; Guo et al., 2020; Sun et al., 2020a). Surface porosity declines, ranging from 3.17% to 24.42% (13.27 average) (Table 3 and Fig. 6(a)). It should be noted that while SEM images of shale samples at different thermal maturity stages can intuitively characterize the evolution of OM pore morphology and structure, several limitations affect accuracy. (i) SEM observation is regional and qualitative to semi-quantitative, making it difficult to comprehensively characterize OM pore development in shale. (ii) Macropores and mesopores can be identified by SEM, whereas micropores cannot be effectively characterized. Researchers have observed and tested the pore structure of kerogen isolates, discussing the relationship between thermal maturity and pores (Craddock et al., 2020; Suekuni et al., 2022). Kerogen can be isolated from shale gas reservoirs through demineralization to remove quartz, feldspar, clay minerals and pyrite, with soluble OM removed by organic solvents (Suleimenova et al., 2014; Craddock et al., 2020; Suekuni et al., 2022). Additionally, critical-point drying is used to replace oven drying to avoid pore collapse caused by the latter method (Sun et al., 2019b; Suekuni et al., 2022). Low-temperature $CO_2$ and $N_2$ adsorption experiments, SEM, and

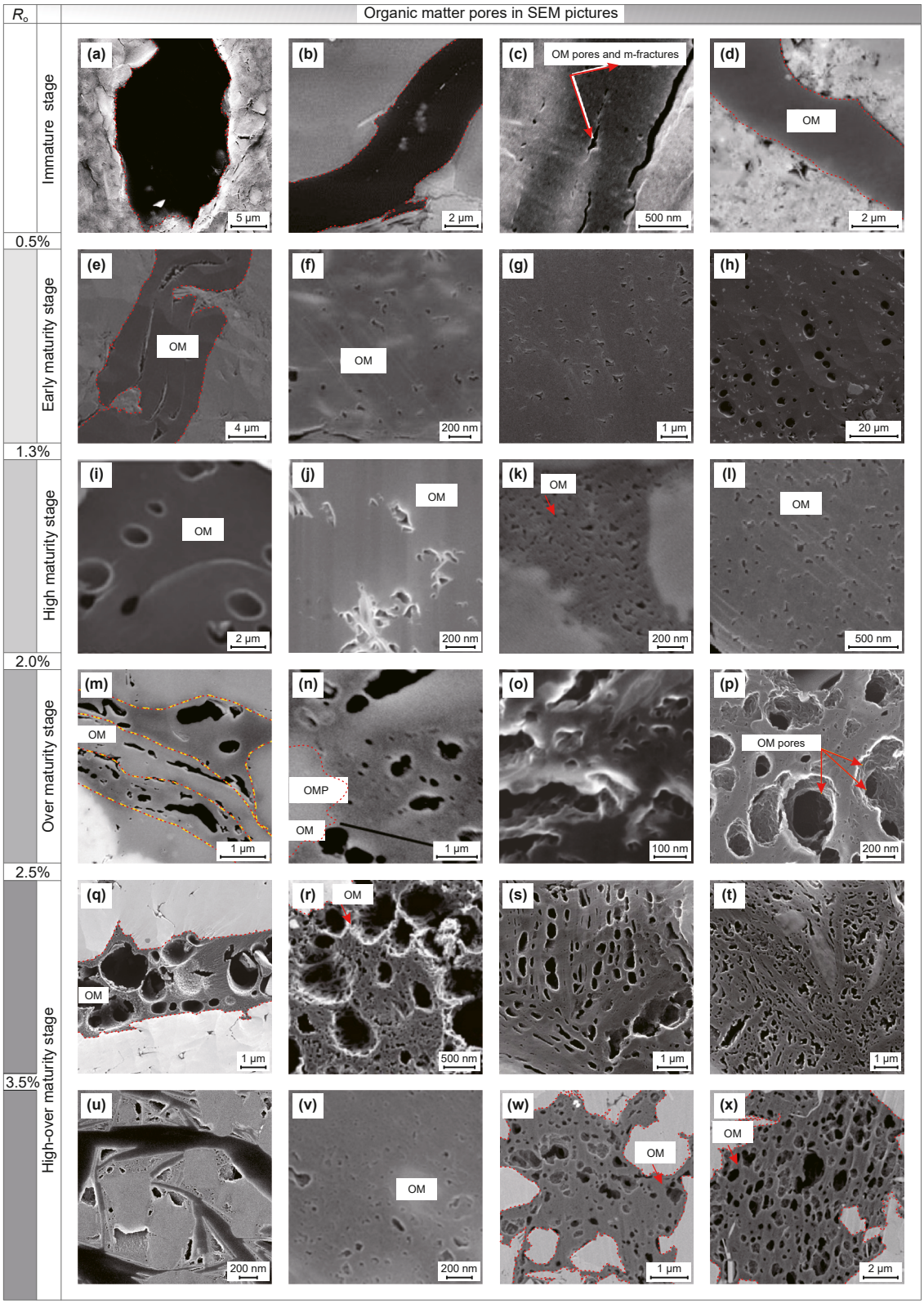


**Fig. 4.** Evolution of OM pores during the hydrocarbon generation in natural maturation series. OM is organic matter, OMP is OM pores. (**a**)–(**d**) reproduced with permission from Liu et al. (2017b), Mastalerz and Schieber (2017) and Shao et al. (2020). OM is immature, some micro-fractures (the length at micron-scale and width at nano-scale) are developed at the edge of OM and a few dissolved pores developed mainly at nano-scale. (**e**)–(**h**) reproduced with permission from Chang et al. (2022), Luo and Zhong (2020), Shao et al. (2020) and Gao et al. (2016). OM is in low maturity stage, some micro-fractures (the length at micron-scale and width at nano-scale) are developed at the edge of OM and certain hydrocarbon generation pores developed at micron to nano scale. (**i**)–(**l**) reproduced with permission from Yu et al. (2022), Iqbal et al. (2021), Shi et al. (2015) and Shao et al. (2020). OM is in high maturity stage, hydrocarbon generation pores developed at micron to nano scale. (**m**)–(**p**) reproduced with permission from Klaver et al. (2015), Park et al. (2021) and Wang et al. (2020c). OM is in over maturity stage, hydrocarbon generation pores widely developed at micron to nano scale. (**q**)–(**x**) reproduced with permission from Chang et al. (2022), Hu et al. (2020a), Yang and Bao (2017), Zhang et al. (2020b) and Sun et al. (2020b). OM is in high-over maturity stage, hydrocarbon generation pores widely developed at micron to nano scale.

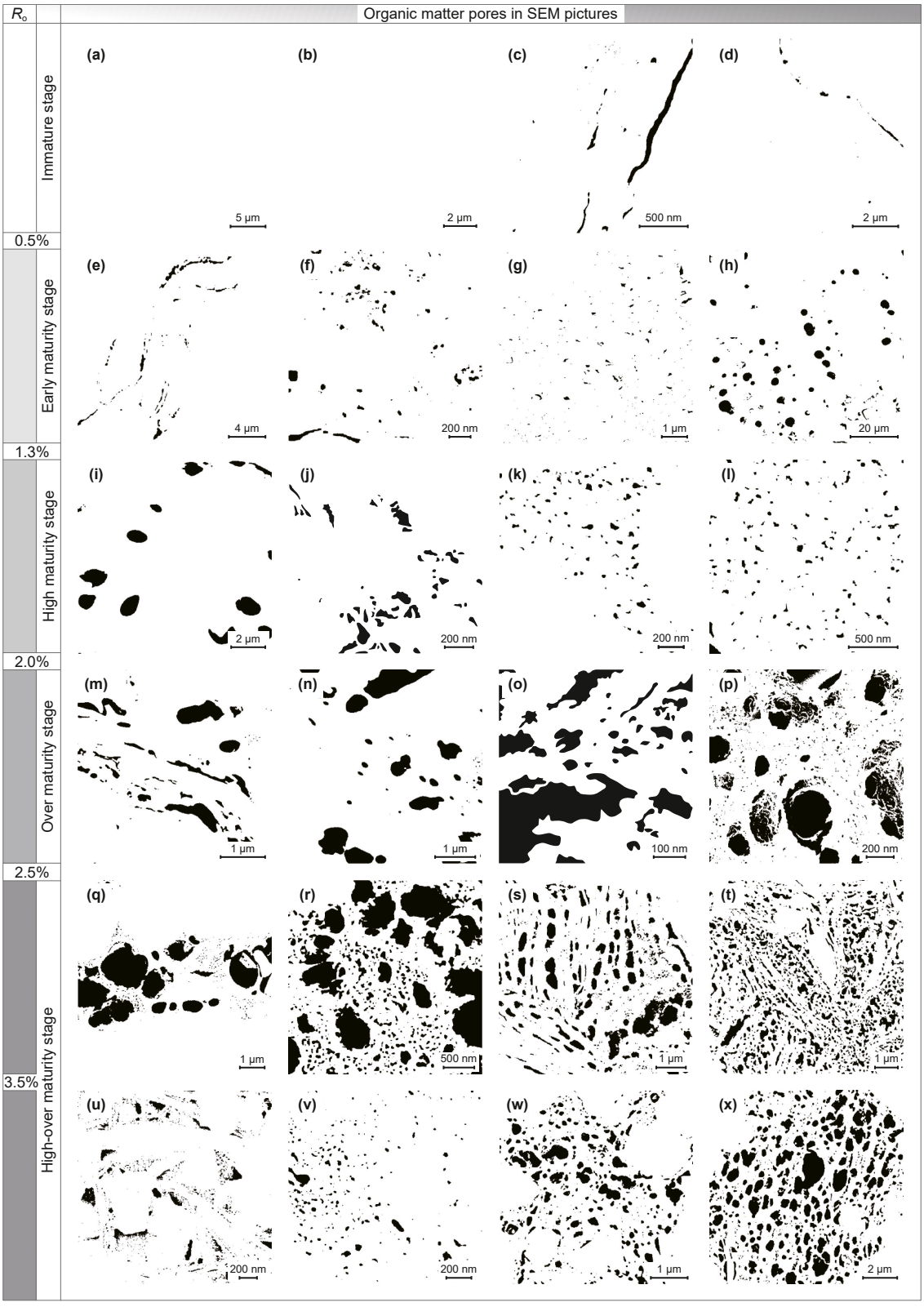


**Fig. 5.** Extraction and surface porosity calculation of OM pores in Fig. 4.

neutron scattering tests were employed to qualitatively and quantitatively characterize the pore structure of kerogen. PV and SSA of kerogen increase, systematically with higher thermal maturity, closely related to the oil and gas generation process (Craddock et al., 2020; Chiang et al., 2020; Suekuni et al., 2022). Note that although various demineralization processes and drying techniques were used to preserve the original morphology, these separation techniques still damaged the original pore structure of kerogen to some extent.

**Table 3**
Surface porosity variation of organic matters in Fig. 4 during natural maturation process.

| Sample ID | SP, % | Sample ID | SP, % | Sample ID | SP, % | Sample ID | SP, % | Sample ID | SP, % | Sample ID | SP, % |
|---|---|---|---|---|---|---|---|---|---|---|---|
| (a) | 0 | (e) | 3.07 | (i) | 5.80 | (m) | 9.15 | (q) | 43.19 | (u) | 5.37 |
| (b) | 0 | (f) | 2.81 | (j) | 6.19 | (n) | 11.72 | (r) | 35.52 | (v) | 3.17 |
| (c) | 2.62 | (g) | 1.04 | (k) | 3.65 | (o) | 29.59 | (s) | 16.17 | (w) | 20.13 |
| (d) | 0.81 | (h) | 4.51 | (l) | 3.25 | (p) | 25.57 | (t) | 19.22 | (x) | 24.42 |
| Average | 0.86 | Average | 2.86 | Average | 4.72 | Average | 19.01 | Average | 28.52 | Average | 13.27 |

SP is surface porosity.

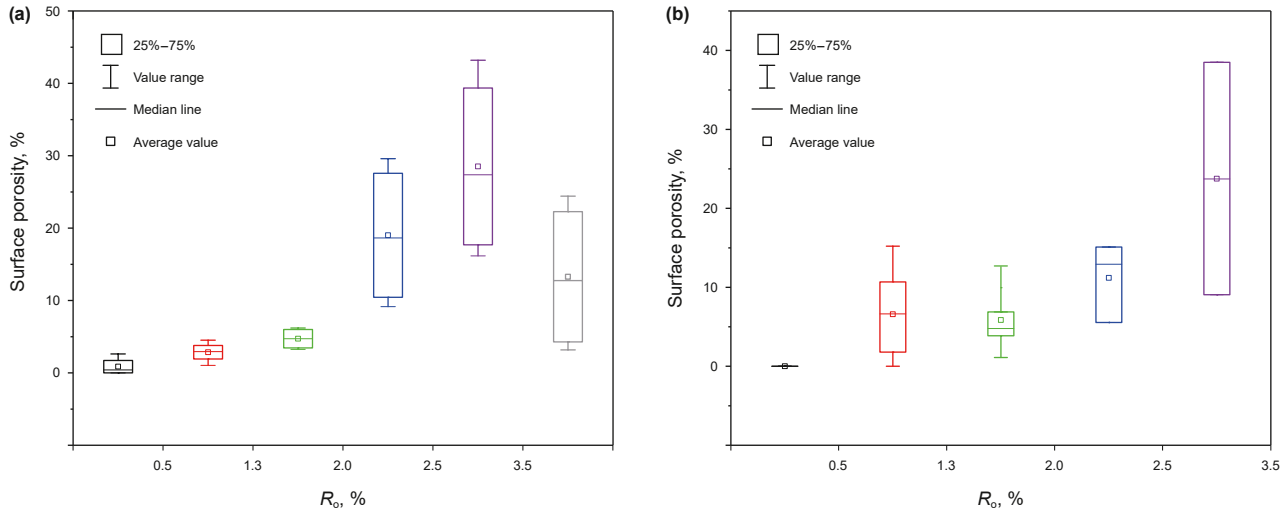


**Fig. 6.** Surface porosity evolution of OM in shale gas reservoirs. (**a**) and (**b**) are in natural and pyrolysis maturation series, respectively.

Moreover, these natural maturation samples were collected from different study areas, with various structural position, sedimentary background, and mineralogical composition, which have significant influence on the pore evolution of shale gas reservoirs. Zhu et al. (2018b) analyzed the relationship between tectonism and pore structure of the Lower Cambrian Lujiaping shale, and indicated that the porosity is positively correlated with brittle deformation, whereas negatively correlated with ductile deformation. Meanwhile, the mixing of OM and inorganic minerals has also an important impact on gas storage and migration pathways, especially for clay minerals. Cheng et al. (2024) stated that the ductile deformation promotes large-aperture transitional pores, mesopores, and small-aperture macropores, but inhibits small-aperture transitional pores, large-aperture macropores, and fracture pores. Yang et al. (2025) investigated the influence of lithofacies on the inflection-point of pore structure evolution, and suggested that the siliceous minerals could effectively prevent OM pore collapsing. Therefore, this kind of lithofacies shale has a slow porosity attenuation compared with other lithofacies. Consequently, the influence of above factors on OM pore evolution in natural maturation samples cannot be avoided, whereas pyrolysis experiments based on the same samples are effective methods.

In addition to SEM observation, high-pressure mercury intrusion and low-temperature gas adsorption experiments were utilized to indirectly characterize the pore structure development in shale gas reservoirs (Tripathy et al., 2019; Mazumder et al., 2024). High-pressure mercury intrusion is advantageous for describing macropores, whereas low-temperature gas adsorption is more suitable for characterizing micropores and mesopores. Cao et al. (2022) combined these technologies to characterize the pore structure parameters of shale gas reservoirs at low maturity, high maturity, and over maturity stages. The PV of these three types of samples ranges from 0.011 to 0.018 $cm^3/g$ (average 0.015 $cm^3/g$), 0.015–0.047 $cm^3/g$ (average 0.031 $cm^3/g$), and 0.004–0.058 $cm^3/g$ (average 0.035 $cm^3/g$), respectively. The SSA ranges from 2.2 to 3.92 $m^2/g$ (average 2.96 $m^2/g$), 6.63–33.12 $m^2/g$ (average 17.55 $m^2/g$), and 2.24–59.67 $m^2/g$ (average 32.02 $m^2/g$), respectively. Both PV and SSA increase with higher maturity. Additionally, the goodness of fit for PV and SSA versus TOC also improves with higher maturity. Xie et al. (2021b) observed a similar phenomenon, indicating that the contribution of OM becomes more significant with higher maturity based on shale samples at different thermal evolution stages. These findings are consistent with statistical results from SEM images, confirming the reliability of the above conclusions through mutual verification.

#### 4.2.2. Evolution of pore structure of OM in pyrolysis experiment series

The continuous evolution of source rock from immature to over mature can be simulated through thermal simulation experiments, which help avoid the influence of differences in diagenetic evolution, mineral composition, and maceral of OM (Topór et al., 2017; Khatibi et al., 2018; Shao et al., 2020; Xu et al., 2021d). This process is extensively used to simulate hydrocarbon generation and pore evolution, especially after the compensation effect of temperature on time in OM pyrolysis was discovered by Waples (1980) and Welte and Tissot (1984). In the simulation system, a rock pyrolysis instrument or thermal simulator is used to simulate the thermal evolution of OM under in-situ strata conditions. A gas chromatograph/mass spectrometer identifies hydrocarbon components, and SEM observes the pore morphology and structural characteristics of shale samples after simulation (Zhou et al., 2018; Correia et al., 2018; Kang et al., 2020). Reaction systems are classified as open, semi-closed, or closed based on their openness (Wu

et al., 2019; Zheng et al., 2020; Song et al., 2021). In an open system, hydrocarbons are immediately discharged upon production; in a closed system, hydrocarbons undergo secondary cracking (Han et al., 2019; Gajica et al., 2022). The semi-closed system, which undergoes episodic hydrocarbon expulsion, closely mimics to the natural evolution of hydrocarbon generation (Cao et al., 2021; Wang et al., 2022). A total of 30 SEM images of shale samples (covering immature to high-over maturity stages) after thermal simulations were collected (Figs. 6 and 7). The corresponding surface porosity of OM pores was also extracted (Table 4), and the evolution of OM pores was discussed. Almost no OM pores were detected in immature shale samples (Figs. 6(p) and 7(p), Table 4). Certain OM pores developed in low maturity shale samples, including micro-factures (with micron-scale length and nano-scale width) and hydrocarbon generation pores (mainly nano-scale) (Fig. 7(a)–(c), (f)–(h), (k)–(m), and (q)). Their surface porosity varied greatly, ranging from 0 to 12.77% (average 6.58%) (Figs. 6(b) and 8(a)–(c), (f)–(h), (k)–(m), and (q), and Table 4). OM pores are well developed in high maturity samples, dominated by hydrocarbon generation pores at micro to nano scale (Fig. 7(d)–(o),

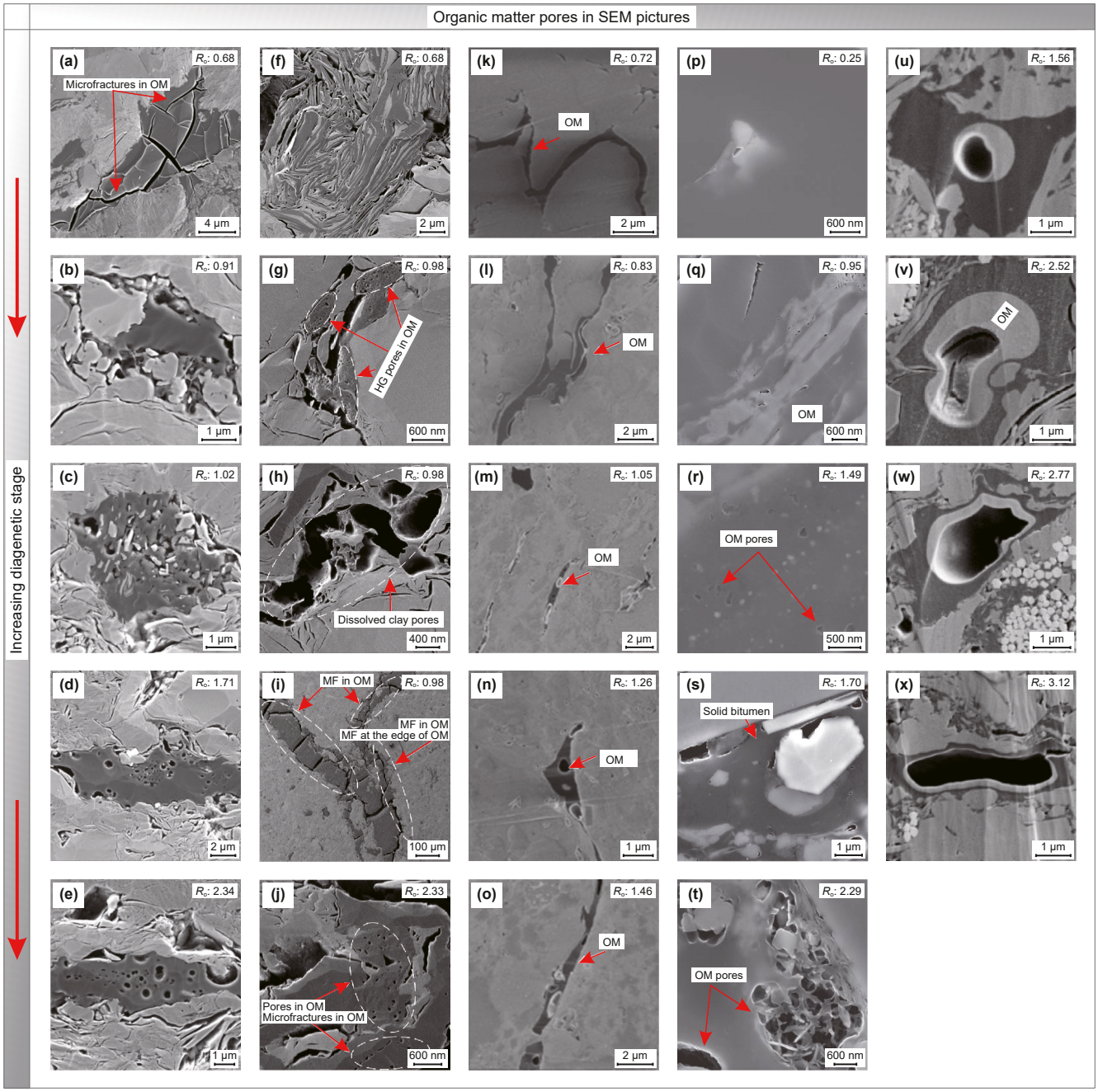


**Fig. 7.** Evolution of OM pores in thermal simulation experiments. OM is organic matter, HG is hydrocarbon generation, and MF is micro-fractures. (**a**)–(**e**) are the Mesoproterozoic Xiamaling Formation shale samples (Yanliao Depression, Northern China) with a type I kerogen, which were reproduced with permission from Shi et al. (2018). (**f**)–(**j**) are Jurassic Yanan Formation shale samples (Western Edge Thrust Belt, Ordos Basin) with a type III kerogen, which were reproduced with permission from Wang and Guo (2019). (**k**)–(**o**) are Paleogene Shahejie Formation shale samples (Dongying Depression, Bohaiwan Basin) with a type $II_1$ kerogen, which were reproduced with permission from Sun et al. (2019b). (**p**)–(**t**) are Devonian to Mississippian New Albany shale samples (Illinois Basin) with a type I or II kerogen, which were reproduced with permission from Valentine et al. (2021). (**q**)–(**x**) are Permian Dalong Formation shale samples (Lower Yangtze Area) with a type I or II kerogen, which were reproduced with permission from Wang and Cao (2016).

**Table 4**
Surface porosity variation of organic matter in Fig. 7 at the evolution process of thermal simulation experiments.

| SID | SP, % | SID | SP, % | SID | SP, % | SID | SP, % | SID | SP, % | Average, % |
|---|---|---|---|---|---|---|---|---|---|---|
| (a) | 8.76 | (f) | 5.66 | (k) | 0 | (p) | 0 | (u) | 3.86 | 0 ($R_o$<0.5 %) |
| (b) | 7.62 | (g) | 12.06 | (l) | 2.61 | (q) | 0.99 | (v) | 9.06 | 6.58 ($R_o$ = 0.5 %–1.3 %) |
| (c) | 3.99 | (h) | 0 | (m) | 12.77 | (r) | 1.11 | (w) | 23.72 | 5.86 ($R_o$ = 1.3 %–2.0 %) |
| (d) | 12.68 | (i) | 9.32 | (n) | 15.22 | (s) | 4.79 | (x) | 38.50 | 11.19 ($R_o$ = 2.0 %–2.5 %) |
| (e) | 15.11 | (j) | 5.55 | (o) | 6.88 | (t) | 12.92 | | | 23.76 ($R_o$ = 2.5 %–3.5 %) |

SID is sample ID, SP is surface porosity.

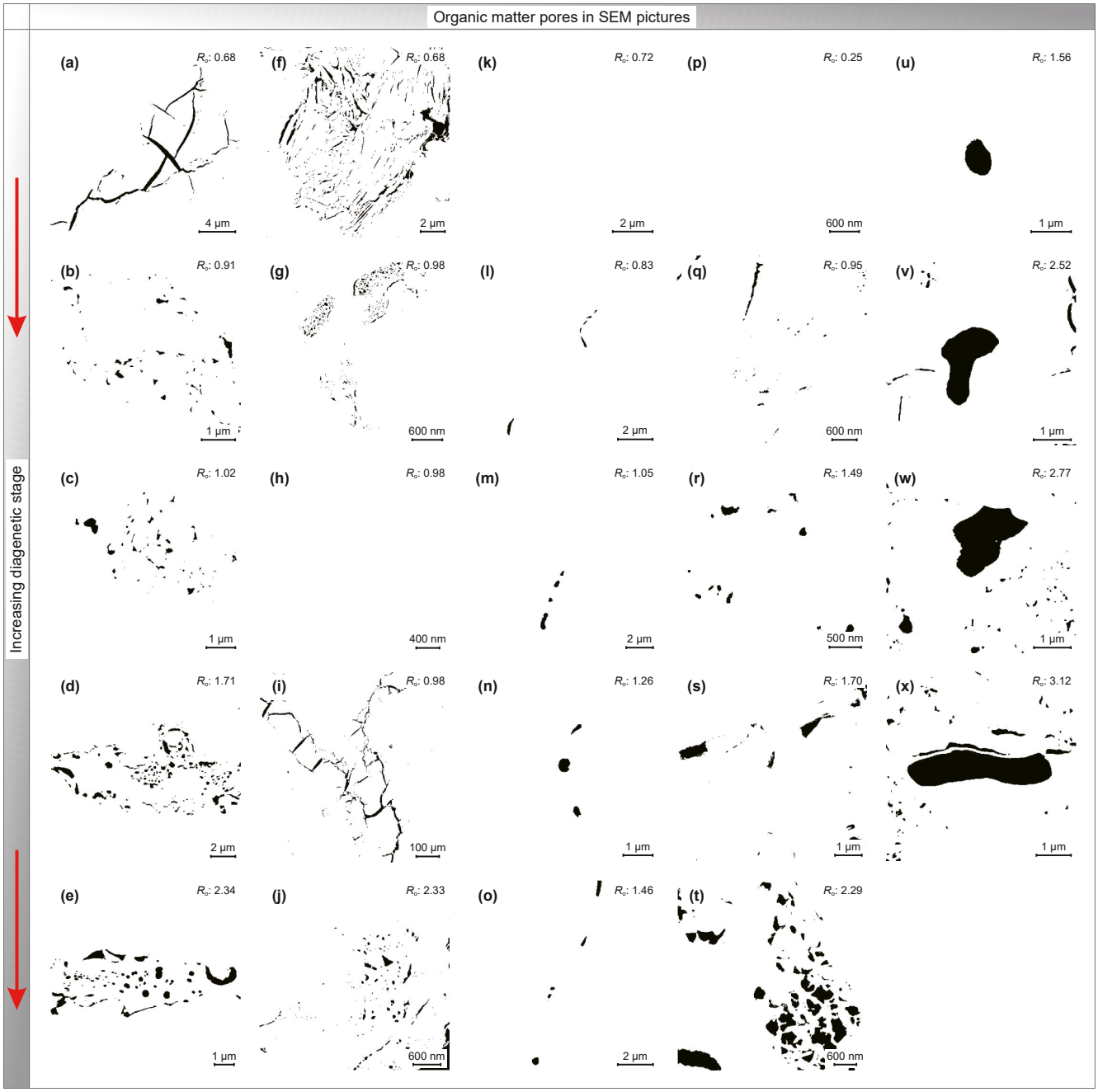


**Fig. 8.** Extraction and surface porosity calculation of OM pores in Fig. 7.

(r), (s), and (u)). Their surface porosity also varied greatly, ranging from 1.11% to 12.68% (average 5.86%) (Figs. 6(b) and 8(d), (o), (r), (s), and (u), and Table 4). In the over maturity stage, hydrocarbon generation pores at nano-scale are widely developed and begin to connect (Fig. 7(e)–(j), and (t)). The surface porosity increases significantly, averaging 11.19% (Figs. 6(b) and 8(e), (j), and

(t), and Table 4). The evolution process in high-over maturity ($R_o$ = 2.5%–3.5%) greatly improves the generation of OM pores, with surface porosity dramatically increasing, ranging from 9.06% to 38.5% (average 23.76%) (Figs. 6(b) and 7(v)–(x) and 8(v)–(x), Table 4). However, the pore structure (mainly reflected in the gradual enlargement of pore size with deeper evolution (Fig. 7(v)–(x))) differs from that in the same stage of natural evolution series (beaded and honeycomb OM pores are densely developed in Fig. 4 (q)–(t)). No SEM images of high-over maturity shale (refers to $R_o$ > 3.5%) were collected in the thermal simulation experiments, but Tan et al. (2021) and Xu et al. (2021d) suggested that pore volume decreases significantly in the high-over maturity stage. Overall, there is a similar pattern in the evolution of OM pores during natural maturation and thermal simulation. However, pore morphology, structure, and surface porosity vary significantly. OM pores in over maturity natural maturation samples are widely developed and interconnected, with greater surface porosity. In contrast, OM pores in thermal simulation samples may develop more centrally, with lower connectivity and surface porosity.

Although thermal simulation experiments have clear advantages in the continuity of OM evolution, some drawbacks affect the accuracy and reliability of the results: (i) high experimental temperatures provide specific compensation for reaction time, but cannot fully offset the negative effects of insufficient pyrolysis and hydrocarbon generation reactions, altering the dynamic process and production components of hydrocarbon generation (Açıkalın, 2011; Valentine et al., 2021). OM pores may develop at a single point rather than multiple points (Fig. 7(u)–(x)). Additionally, the surface porosity of OM in thermal simulations is generally lower than that of natural maturation shale samples (Tables 3 and 4). (ii) The dynamic characteristics and coupled effects of temperature and pressure in real shale gas reservoirs are ignored, as experiments are usually conducted at a fixed pressure. (iii) The influence of diagenesis (mechanical compaction, dissolution, and cementation) on OM pores and mineral catalysis (mainly smectite and illite) on the hydrocarbon generation process is not fully considered. (iv) It is challenging to set the hydrocarbon expulsion amount and process in the semi-closed system to accurately reflect the real geological history. (v) There are significant differences in $R_o$ corresponding to the same experimental temperature in different studies (Ma et al., 2017b; Shi et al., 2018), leading to distinct development characteristics of OM pores. (vi) Shale samples are prone to rupture due to high temperature and pressure during thermal simulations (Sun et al., 2017; Qu et al., 2017), complicating SEM sample preparation for pore observation. Dynamic experimental temperature, pressure, and other environmental conditions could be set according to paleoenvironment and the physicochemical properties of the water medium, better simulating the influence of hydrocarbon generation and diagenesis on the evolution of OM pores in the real diagenetic process.

Reaction systems of pyrolysis experiments include open, semi-closed, and closed based on their openness (Wu et al., 2019; Zheng et al., 2020; Song et al., 2021). In an open system, hydrocarbons are immediately discharged upon production, which was mostly used to analyze the maturity and porosity evolution; semi-closed system is available to describe the episodic hydrocarbon expulsion of OM; and closed system can well characterize the secondary cracking of hydrocarbons (Han et al., 2019; Cao et al., 2021; Gajica et al., 2022; Wang et al., 2022). Moreover, the differences in aqueous or anhydrous pyrolysis, the parameters setting of temperature points, heating rate, simulation time and pressure, also lead to different evolution processes of OM pores (Sun et al., 2019b; Shao et al., 2020; Hou et al., 2025). Besides, OM in their pyrolysis experimental shale samples comprises type I, II, and III kerogen, with the former two were mainly developed in marine and continental shale gas reservoirs, and the last was mostly found in marine-continental transitional reservoirs. Besides the influence of thermal maturity, different types of OM with diverse chemical structure impact also crucially to the pore structure (Ungerer et al., 2015; Tian et al., 2017). According to the ratio of H and C, and O and C, OM is divided into four types of I (mainly from various types of algae, H/C > 1.25 and O/C < 0.15), II (mainly from marine planktonic organisms, H/C < 1.25 and O/C in the range of 0.03–0.18), III (mainly from higher plant, H/C < 1 and O/C in the range of 0.03–0.3), and IV (mainly polycyclic aromatic hydrocarbons, and H/C < 0.5), and shale gas reservoirs mainly contain the former three (Van Krevelen, 1950, 1984; Ma et al., 2018; Donadelli et al., 2019). Type I and II kerogen are prone to generating a lot of liquid hydrocarbons and partial are remained in shale pores. Subsequently, with deepening thermal evolution, the remained liquid hydrocarbons undergo secondary cracking to form a large amount of gas, leading to rapid expansion of pore space in OM and the formation of OM pores (Barker, 1990; Zhang et al., 2014). On the other hand, Tian et al. (2017) and Huang et al. (2018) suggested that the structure pore inner type III kerogen is the most developed, which is different from the trend of hydrocarbon generation pores. Additionally, higher TOC usually corresponds to more developed nano pores, which influences the pore size distribution and enhances the connectivity and surface complexity of OM pores (Guo et al., 2015; Yang et al., 2019). Yang et al. (2014, 2016b) indicated that the fractal dimension of shale pores is mainly in the range of 2.68–2.83, and a higher TOC is conducive to a larger fractal dimension. They stated that TOC improves the develop of PV and SSA, especially for micropores, and decreases the pore diameter. Hence, rougher pore surfaces and more complex pore structure are formed. Also, its adsorption capacity to $CH_4$ is higher (Yang et al., 2014; Yang et al., 2016b). Although the pyrolysis experimental results were combined controlled by experimental parameters, and the compositional and structural differences in OM, the general hydrocarbon generation and pore forming evolution trends are consistent.

### 4.3. Controlling mechanism of hydrocarbon generation evolution on the pore structure of OM

Thermal maturity comprehensively reflects the changes in the chemical and physical properties of OM during diagenesis process, controlling hydrocarbon generation and the evolution of OM pores in shale (Bohacs et al., 2013; Tang et al., 2019). Therefore, the hydrocarbon generation pattern is summarized (Fig. 9), clarifying the types of hydrocarbon generation, byproducts, mechanisms, and corresponding OM pores at each stage. In the immature stage, the evolution temperature is roughly below 60 °C, and hydrocarbon generation is dominated by biochemical process (mainly gelification and condensation, with reduction bacteria and other microorganisms playing a significant role) (Barnes et al., 1984; Dai and Jiang, 1990; Ding et al., 2003; El-Habaak et al., 2020). Biogas, immature oil, and kerogen aromatic skeleton are generated at this stage (Liang, 1985; Wang, 2000; Miao et al., 2017). As diagenetic evolution progresses, biochemical processes gradually transition to geochemical processes (Rice and Claypool, 1981; Rohrback et al., 1984). Hydrocarbon generation pores are not well developed at this stage, with shrinkage micro-fractures being dominant (Sun et al., 2022; Faboya et al., 2020). Additionally, a certain number of primary pores (biological structure pores) are also developed (Tenger et al., 2021). In the low maturity stage, the evolution temperature ranges from 50 to 150 °C, and thermal degradation/thermal catalysis (including bitumization and aromatization) is the dominant hydrocarbon generation mechanism (Carr, 1999; Miskolczi and Nagy, 2012). Liquid bitumen is cracked into oil,

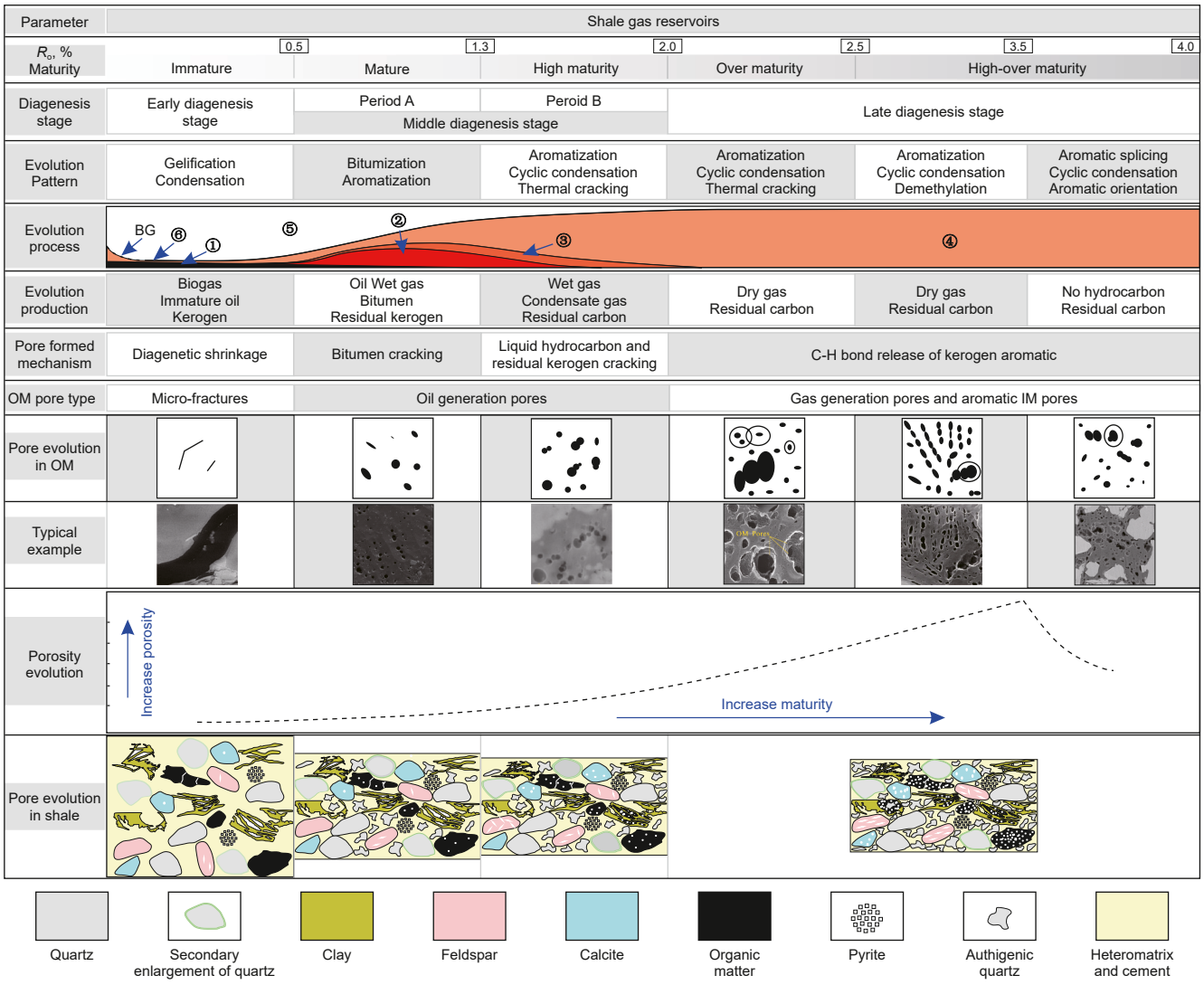


**Fig. 9.** Hydrocarbon generation and OM pores evolution pattern during thermal evolution process. BG is biogas, OM is organic matter, IM is inter-molecular, and MF is micro-fracture. ① is original bitumen, hydrocarbon, and non-hydrocarbon compounds; ② is oil; ③ is wet gas and condensate gas; ④ is gaseous hydrocarbon, including wet gas, condensate gas, and dry gas; ⑤ is kerogen, which is gradually transformed into residual carbon in the thermal evolution process; ⑥ is immature oil.

wet gas, and aromatic skeleton, with oil generation pores being the dominant pore type (Goodarzi et al., 1992; Cardott et al., 2015; Gao et al., 2020). In the high maturity stage, the evolution temperature ranges from 150 °C to 200 °C, and hydrocarbon generation is dominated by aromatization, cyclic condensation, and thermal cracking (Jochum, 2000; Rodriguez and Philp, 2010). Small molecular hydrocarbons are generated by the thermal degradation of kerogen (Li et al., 2016; Huang et al., 2017). Additionally, gaseous hydrocarbons are generated by the thermal cracking (the release of C-C bond) of residual oil, as reservoir temperatures exceed the critical temperature of liquid hydrocarbons (Wenger et al., 2002; Zhang et al., 2015b), with residual carbon being the main solid product. Wet gas and condensate gas are formed at this stage, and gas generation pores are relatively well developed. Furthermore, isolated OM pores begin to show signs of connectivity (Fig. 4(j)–(l)).

In the over maturity stage, reservoir temperatures exceed 200 °C (Ye et al., 2017; Fu et al., 2019). Aromatization, cyclic condensation, and thermal cracking dominate OM evolution. Most side chains and groups on kerogen that can be broken have disappeared, and long-chain liquid hydrocarbons can no longer be generated (Welte and Tissot, 1984; MacGowan et al., 1993). Dry gas is generated by the thermal cracking of short alkyl branched chains connected to the aromatic structure (the release of C-H bond of kerogen aromatics), with residual carbon as the corresponding solid product (Zhang et al., 2011; Fang et al., 2012; Miao et al., 2017). Additionally, some gas is formed by cracking liquid hydrocarbons (Zheng et al., 2020; Su et al., 2021). Gas generation pores are well developed at this stage, with a dramatic increase in surface porosity (Tables 3 and 4). The connectivity of OM pores is significantly improved, with interconnected OM pores and numerous micropores developed within macropores in a mosaic structure (Fig. 4(m)–(p)). In the high-over maturity stage ($R_o$ = 2.5%–3.5%), demethylation is the primary method of dry gas generation, reaching the peak of gas generation (Peng et al., 2020; Tan et al., 2021; Horsfield et al., 2021). OM pores are extremely well developed, with average surface porosity significantly increasing to 28.52% (Table 3). Beaded connected OM pores form an interconnected three-dimensional pore network (Fig. 4(q)–(t)). Beyond this stage ($R_o$ > 3.5%), hydrocarbons are no longer generated (Xiao et al., 2015b; Pang et al., 2020). Excessively high thermal maturity fundamentally changes the structure of OM, including

further polycondensation of kerogen, cyclic condensation and structural reorganization of OM, increased fused aromatic ring system (splicing action), enhancd of macromolecular orientation, and a trend towards graphitization (orientation action) (Liu et al., 2013b; Tenger et al., 2021). Consequently, the source rock enters an open state with high hydrocarbon expulsion efficiency, the lattice defects in OM are gradually reduced, the disordered structure of aromatic nuclei transforms into the ordered structure of graphite crystals, the kerogen structure becomes orderly and compact, OM pores are reduced, pore structure worsens, and adsorption heat sharply decreases, resulting in a poorer gas-bearing capacity (Wang et al., 2020c; Cao et al., 2021). The graphite peak appears in the Raman spectrum of OM, and internal pores gradually disappear when $R_o > 4.0\%$ (Liu et al., 2013b; Wang et al., 2018; Tenger et al., 2021). The average surface porosity of OM significantly declines to 13.27% in natural maturation samples (Table 3).

The hydrocarbon generation and oil and gas filling processes of different source rocks - reservoirs exhibit strong heterogeneity controlled by variations in kerogen types and macerals (Makeen et al., 2020; Luo et al., 2021; Thana'Ani et al., 2022). There are obvious differences in the macerals of different types of kerogen, and even within the same type of kerogen, macerals show strong heterogeneity (Abarghani et al., 2020; Gonciaruk et al., 2021). The hydrocarbon generation potential, types, threshold, oil-gas ratio, and maximum hydrocarbon production rate of each maceral vary. Sapropelic and exinite macerals have the greatest hydrocarbon generation potential, vitrinite is conducive to gas generation, whereas inertinite has poor hydrocarbon generation potential (Zhang et al., 2018b; Xu et al., 2018). Vitrinite content in type III kerogen (mainly from higher plants) is significantly higher than in type I and II kerogen (mainly from various types of algae and marine planktonic organisms) (Van Krevelen, 1950, 1984; Ma et al., 2018; Donadelli et al., 2019), as confirmed by the calculation of the TI index (Xie et al., 2022b). Consequently, the PV and SSA are more developed, and adsorption capacity of type III kerogen is higher in experimental and molecular simulation results. A dynamic hydrocarbon generation pattern is still lacking, which can automatically adjust to the most suitable hydrocarbon generation pattern based on the maceral or atomic composition of OM.

### 4.4. Evolution pattern of OM pores during thermal maturation

Based on the content above, the role of OM in shale pore structure and adsorption capacity varies with the thermal evolution process, which is controlled by the evolution of structure and pores. Porosity and pore connectivity change significantly with higher thermal maturity of OM. The evolution pattern of hydrocarbon generation and OM pores, the corresponding hydrocarbon generation mechanism, and the evolution process of total porosity in shale are summarized to reveal the evolution of the adsorption capacity and the controlling factors (Fig. 9).

In immature shale gas reservoirs, hydrocarbon generation pores of OM are poorly developed, with only a few primary structural pores and diagenetic shrinkage micro-fractures observed (Fig. 4(a)–(d)). Therefore, the contribution of TOC to the adsorption capacity of shale is weak (Fig. 3). Xie et al. (2022a) suggested that clay mineral content dominates the adsorption capacity of shale due to the widely developed intergranular and intragranular pores. In low maturity shale gas reservoirs, significant amounts of liquid hydrocarbons are generated. Although the generation of liquid hydrocarbons is accompanied by the formation of OM pores, these pores are often filled with new OM, resulting in reduced porosity and making them difficult to identify (Nie et al., 2019b; Li et al., 2020c, 2022). Overall, the surface porosity of OM pores is slightly improved at this stage. Generally, the adsorption capacity of shale is dominated by primary mineral pores, with TOC playing a non-essential role (Fig. 3). In high maturity shale gas reservoirs, gaseous hydrocarbons (wet gas and condensate gas) begin to be generated in large quantities. A large number of hydrocarbon generation pores are formed by the thermal cracking of residual kerogen and liquid hydrocarbons, gradually improving surface porosity of OM pores. Moreover, the loss of primary mineral pores in shale is significant, and the adsorption capacity of shale becomes controlled by TOC. Additionally, OM pores begin to connect with each other, which is crucial for the enrichment and migration of shale gas (Fig. 4(i)–(m)). In over maturity shale gas reservoirs, the C-H bonds in kerogen aromatics are broken, forming large amounts of dry gas through thermal cracking. Gas generation pores are widely developed at this stage, significantly increasing surface porosity of OM. The connectivity of OM pores is further enhanced, and the influence of TOC on the adsorption capacity of shale is also improved. In high-over maturity ($R_o = 2.5\%–3.5\%$) shale gas reservoirs, the peak of dry gas generation is reached, promoted by the demethylation of residual kerogen. The surface porosity and connectivity of OM pores are the best, with beaded interconnected OM pores and "mosaic type" OM pores widely developed. Consequently, the contribution of TOC to the adsorption capacity of shale reaches its peak at this stage. However, after $R_o > 3.5\%$, the degree of OM aromatization becomes too high, reducing the sealing properties and decreasing the number of OM pores, which may even disappear. Consequently, the adsorption capacity of OM dramatically declines at this stage. Overall, $R_o$ of 3.5% is regarded as the limit for hydrocarbon generation and $R_o$ of 4.0% is the limit of OM pores (Chen and Xiao, 2014; Wang et al., 2018; Tenger et al., 2021).

## 5. Current challenges and research prospects

(1) The accuracy and precision of the isothermal adsorption experiments are affected by several issues. (i) Crushed or ground particle samples may have their pore structure damaged, which may not fully represent real continuous shale gas reservoirs. (ii) Errors in the calculation process and results of sample volume/mass, blank test, buoyancy test, and free volume test are characterized by uncontrollability. (iii) Isothermal adsorption experiments are mostly performed at a fixed temperature, ignoring the dynamics of temperature and pressure in real shale gas reservoirs and their coupled control on the adsorption process. (iv) In the correction process of absolute adsorption capacity, various methods to obtain the adsorption phase density and bulk density yield distinct calculation results, and an authoritative scheme is lacking. Consequently, an isothermal adsorption experiment of bulk shale samples covering the dynamic conditions of temperature and pressure is urgently needed. Additionally, an intuitive quantitative test method for gas density in the adsorption system is also crucial, with Neutron Scattering Spectrometer showing great potential.

(2) In isothermal adsorption experiments: (i) the discussion of the contribution of TOC to adsorption capacity is based on intact shale, and the influence of mineral composition cannot be avoided. (ii) Shale samples from different basins are characterized by high heterogeneity, resulting in differences in hydrocarbon generation potential, OM pore development, and adsorption capacity. Additionally, the sealing ability of source rock - reservoir and the evolution process of OM pores are distinct. (iii) The macerals of shale samples with different sedimentary backgrounds are distinct, leading to different hydrocarbon generation and pore forming abilities. Shale samples selected from the same formation of

the same sedimentary basin may exhibit a gradation feature due to differences in tectonic subsidence or proximity to magmatic intrusion areas. Therefore, the contribution of TOC to shale adsorption capacity at different thermal evolution stages can be better reflected. The hydrocarbon generation patterns and oil and gas filling processes exhibit strong heterogeneity in different types of kerogen and macerals, resulting in different hydrocarbon generation potential, types, thresholds, oil-gas ratios, and maximum hydrocarbon production rates. There is a lack of a dynamic hydrocarbon generation pattern that can automatically adjust to the most suitable hydrocarbon generation pattern for OM with different macerals.

(3) Pore damage caused by the isolation of kerogen: PV, SSA, and adsorption capacity of kerogen are functions of thermal maturity, closely related to the generation process of oil and gas. (i) Extracting kerogen from shale gas reservoirs with different maturity and characterizing the evolution process of pore type, morphology, size, connectivity, PV, SSA, etc. through experiments such as visual observation, scanning, and liquid injection are currently the most intuitive and closest to the natural evolution process. However, this complex step involves multiple procedures, increasing the potential for errors. (ii) Demineralization for removing quartz, feldspar, clay minerals and pyrite, even soluble OM, may lead to changes in the pore structure of OM, such as the re-freeing of pores filled by minerals and the dissolution of soluble OM to form new pores. Additionally, the original morphology of kerogen is also changed. (iii) Oven drying used in the isolation process causes pore collapse in kerogen, while critical-point drying has been proven to mitigate this to some extent. Although various demineralization processes and drying techniques are used to obtain the original morphology of kerogen, these separation techniques still damage the original pore structure of kerogen to some content. A comprehensive instrument capable of observing and identifying different components of integral shale, as well as corresponding pore structures and $CH_4$ adsorption characteristics, is expected to solve these problems.

(4) Several disadvantages of thermal simulation experiments of OM pores need to be addressed: (i) insufficient pyrolysis and hydrocarbon generation reaction, and the dynamic process and production components of hydrocarbon generation are altered by the short pyrolysis times. Additionally, the pore development of OM in thermal simulation samples is slightly lower than that of natural maturation shale samples. (ii) The coupled effect of temperature and pressure in real shale gas reservoirs cannot be fully replicated in thermal simulation experiments, and the influence of diagenesis and the mineral catalysis on hydrocarbon generation and OM pore formation also needs to be considered. (iii) During the construction of semi-closed experimental systems, setting the hydrocarbon expulsion amount and process to match the real geological process is challenging. Additionally, the thermal maturity of OM and the development of OM pores corresponding to the same simulated temperature vary significantly in different experiments. (iv) Shale samples may break during the thermal simulation process, especially at high temperatures and pressures, complicating subsequent supporting experiments. A high-precision thermal simulation experiment is urgently needed, considering the dynamic experimental temperature, pressure, and other environmental conditions of real shale gas reservoirs.

## 6. Conclusion

(1) OM pores are significant accumulation spaces for shale gas. Primary OM pores consist of biological reticular fiber structures, cell cavities, animal cavities, and intermolecular microfractures. Secondary OM pores are mainly hydrocarbon generation pores, along with certain dissolved pores formed by the dissolution of organic acids. As thermal evolution progresses, primary pores gradually disappear, and secondary OM pores form the foundation of the pore network system in shale gas reservoirs. In immature and low maturity shale, the contribution of TOC to adsorption amount is inconspicuous, with no significant positive correlation recorded. In contrast, since the high maturity stage, the adsorption capacity of shale is dominated by TOC, exhibiting a clear positive linear correlation between TOC and adsorption capacity. From natural maturation shale samples and thermal simulation experiments, the surface porosity of OM in SEM images gradually increases with higher maturity, reaching a peak at the high-over maturity stage ($R_o$ = 2.5%–3.5%). It then declines with further thermal evolution.

(2) The development of OM pores is controlled by thermal evolution and hydrocarbon generation processes. In immature shale, OM pores are poorly developed, with OM evolution driven by biochemical action at this stage. Only a small amount of immature oil and biogas is formed, contributing weakly to pore development. In low maturity shale, a large number of liquid hydrocarbons are generated, accompanied by the formation of OM pores, but also filling some pores. The surface porosity of OM rises slightly. From high maturity to high-over maturity stages, gaseous hydrocarbons are generated in large quantities, gradually reaching a peak. Correspondingly, gas generation pores are extensively developed within OM, and beaded interconnected and “mosaic type” OM pores are widely developed, greatly improving the connectivity of the pore system and the gas-bearing capacity of shale gas reservoirs. However, the development of OM pores deteriorates for $R_o$ values higher than 3.5%, and the graphitization trend is not conducive to the preservation of OM pores.

## CRediT authorship contribution statement

**Wei-Dong Xie:** Software, Writing – original draft, Data curation, Writing – review & editing, Methodology. **Xiao-Fei Fu:** Writing – review & editing, Writing – original draft. **Hai-Xue Wang:** Writing – original draft. **Yu Sun:** Writing – original draft. **Veerle Vandeginste:** Writing – review & editing. **Xiao-Peng Li:** Validation, Software.

## Declaration of competing interest

The authors declare no competing financial interest.

## Acknowledgements

The authors gratefully acknowledge the supports of the National Natural Science Foundation of China (No. U19B2007, 42072202), and the China Postdoctoral Science Foundation (No. 2025MD774057).

## References


Abarghani, A., Gentzis, T., Shokouhimehr, M., Liu, B., Ostadhassan, M., 2020. Chemical heterogeneity of organic matter at nanoscale by AFM-based IR spectroscopy. Fuel 261, 116454. https://doi.org/10.1016/j.fuel.2019.116454.

Açıkalın, K., 2011. Thermogravimetric analysis of walnut shell as pyrolysis feedstock. J. Therm. Anal. Calorim. 105 (1), 145–150. https://doi.org/10.1007/s10973-010-1267-x.

Aji, A.Q.M., Mohshim, D.F., Maulianda, B., Elraeis, K.A., 2022. Supercritical methane adsorption measurement on shale using the isotherm modelling aspect. RSC Adv. 12 (32), 20530–20543. https://doi.org/10.1039/D2RA03367D.

Awan, R.S., Liu, C., Yasin, Q., Liu, B., Wood, D.A., Feng, D., Wu, Y., Iltaf, K.H., 2024. Geologic characterization of the lower Paleozoic black shale of the Niutitang Formation: Implications for a shale gas potential in Western Hunan, China. Mar. Petrol. Geol. 163, 106756. https://doi.org/10.1016/j.marpetgeo.2024.106756.

Bakshi, T., Vishal, V., 2021. A review on the role of organic matter in gas adsorption in shale. Energy Fuels 35 (19), 15249–15264. https://doi.org/10.1021/acs.energyfuels.1c01631.

Bakshi, T., Prusty, B.K., Pathak, K., Pal, S.K., 2018. Pore characteristics of damodar valley shale and their effect on gas storage potential. J. Petrol. Sci. Eng. 162, 725–735. https://doi.org/10.1016/j.petrol.2017.10.091.

Bao, Y., Ju, Y., Yin, Z., Xiong, J., Wang, G., Qi, Y., 2020. Influence of reservoir properties on the methane adsorption capacity and fractal features of coal and shale in the upper Permian coal measures of the South Sichuan coalfield, China. Energy Explor. Exploit. 38 (1), 57–78. https://doi.org/10.1177/0144598719877527.

Barker, C., 1990. Calculated volume and pressure changes during the thermal cracking of oil to gas in reservoirs. AAPG (Am. Assoc. Pet. Geol.) Bull. 74 (8), 1254–1261. https://doi.org/10.1306/0C9B247F-1710-11D7-8645000102C1865D.

Barnes, M., Barnes, W., Bustin, R., 1984. Diagenesis 8. Chemistry and evolution of organic matter. Geosci. Can. 11 (3), 103–114. https://id.erudit.org/iderudit/geocan11_3art01.

Baruch, E.T., Kennedy, M.J., Löhr, S.C., Dewhurst, D.N., 2015. Feldspar dissolution-enhanced porosity in Paleoproterozoic shale reservoir facies from the barney creek formation (McArthur Basin, Australia). AAPG (Am. Assoc. Pet. Geol.) Bull. 99 (9), 1745–1770. https://doi.org/10.1306/04061514181.

Bohacs, K.M., Passey, Q.R., Rudnicki, M., Esch, W.L., Lazar, O.R., 2013. The spectrum of fine-grained reservoirs from shale gas to shale oil/tight liquids: essential attributes, key controls, practical characterization. In: IPTC 2013: International Petroleum Technology Conference. European Association of Geoscientists & Engineers, p. 350. https://doi.org/10.3997/2214-4609-pdb.350.iptc16676.

Boruah, A., Rasheed, A., Mendhe, V.A., Ganapathi, S., 2019. Specific surface area and pore size distribution in gas shales of Raniganj Basin, India. J. Pet. Explor. Prod. Technol. 9 (2), 1041–1050.

Bowker, K.A., 2007. Barnett shale gas production, Fort Worth Basin: issues and discussion. AAPG (Am. Assoc. Pet. Geol.) Bull. 91 (4), 523–533. https://doi.org/10.1306/06190606018.

Bu, H., Ju, Y., Tan, J., Wang, G., Li, X., 2015. Fractal characteristics of pores in non-marine shales from the Huainan coalfield, eastern China. J. Nat. Gas Sci. Eng. 24, 166–177. https://doi.org/10.1016/j.jngse.2015.03.021.

Cao, T., Deng, M., Cao, Q., Huang, Y., Yu, Y., Cao, X., 2021. Pore formation and evolution of organic-rich shale during the entire hydrocarbon generation process: examination of artificially and naturally matured samples. J. Nat. Gas Sci. Eng. 93, 104020. https://doi.org/10.1016/j.jngse.2021.104020.

Cao, T., Liu, H., Pan, A., Fu, Y., Deng, M., Cao, Q., Huang, Y., Yu, Y., 2022. Pore evolution in siliceous shales and its influence on shale gas-bearing capacity in eastern Sichuan-western Hubei, China. J. Petrol. Sci. Eng. 208, 109597. https://doi.org/10.1016/j.petrol.2021.109597.

Cardott, B.J., Landis, C.R., Curtis, M.E., 2015. Post-oil solid bitumen network in the Woodford Shale, USA—A potential primary migration pathway. Int. J. Coal Geol. 139, 106–113. https://doi.org/10.1016/j.coal.2014.08.012.

Carr, A.D., 1999. A vitrinite reflectance kinetic model incorporating overpressure retardation. Mar. Petrol. Geol. 16 (4), 355–377. https://doi.org/10.1016/S0264-8172(98)00075-0.

Carter, K.M., Harper, J.A., Schmid, K.W., Kostelnik, J., 2011. Unconventional natural gas resources in Pennsylvania: the backstory of the modern Marcellus Shale play. Environ. Geosci. 18 (4), 217–257. https://doi.org/10.1306/eg.09281111008.

Cavelan, A., Boussafir, M., Rozenbaum, O., Laggoun-Défarge, F., 2019. Organic petrography and pore structure characterization of low-mature and gas-mature marine organic-rich mudstones: insights into porosity controls in gas shale systems. Mar. Petrol. Geol. 103, 331–350. https://doi.org/10.1016/j.marpetgeo.2019.02.027.

Chandra, D., Bakshi, T., Bahadur, J., Hazra, B., Vishal, V., Kumar, S., Sen, D., Singh, T. N., 2023. Pore morphology in thermally-treated shales and its implication on CO2 storage applications: a gas sorption, SEM, and small-angle scattering study. Fuel 331, 125877. https://doi.org/10.1016/j.fuel.2022.125877.

Chandra, A., Sarkar, P., Singh, K.H., Singh, T.N., 2025. A comprehensive study on pore topology of Lower Indian Gondwana shale using pore-scale 2D scan electron micrographs. J. Earth Syst. Sci. 134 (1), 57.

Chang, J., Fan, X., Jiang, Z., Wang, X., Chen, L., Li, J., Zhu, L., Wan, C., Chen, Z., 2022. Differential impact of clay minerals and organic matter on pore structure and its fractal characteristics of marine and continental shales in China. Appl. Clay Sci. 216, 106334. https://doi.org/10.1016/j.clay.2021.106334.

Chen, J., Xiao, X., 2014. Evolution of nanoporosity in organic-rich shales during thermal maturation. Fuel 129, 173–181. https://doi.org/10.1016/j.fuel.2014.03.058.

Chen, Y., Wei, L., Mastalerz, M., Schimmelmann, A., 2015. The effect of analytical particle size on gas adsorption porosimetry of shale. Int. J. Coal Geol. 138, 103–112. https://doi.org/10.1016/j.coal.2014.12.012.

Chen, L., Jiang, Z., Liu, K., Tan, J., Gao, F., Wang, P., 2017. Pore structure characterization for organic-rich Lower Silurian shale in the upper yangtze platform, South China: a possible mechanism for pore development. J. Nat. Gas Sci. Eng. 46, 1–15. https://doi.org/10.1016/j.jngse.2017.07.009.

Chen, X., Guo, T., Shi, D., Hou, Q., Wang, C., 2019. Pore structure characteristics and adsorption capacity of Niutitang formation shale in southern Shaanxi. Lithologic Reservoirs 31, 52–60.

Chen, F., Zheng, Q., Ding, X., Lu, S., Zhao, H., 2020a. Pore size distributions contributed by OM, clay and other minerals in over-mature marine shale: a case study of the longmaxi shale from Southeast Chongqing, China. Mar. Petrol. Geol. 122, 104679. https://doi.org/10.1016/j.marpetgeo.2020.104679.

Chen, G., Lu, S., Liu, K., Xu, C., Xue, Q., Tian, S., Li, J., Lu, S., Zhang, Y., 2020b. Occurrence state and micro mechanisms of shale gas on pore walls. Earth Sci. 45 (5), 1782–1790.

Cheng, G., Wu, C., Jiang, B., Li, F., Li, M., Song, Y., 2024. Pore structure evolution of organic-rich shale induced by structural deformation based on shale deformation experiments. Energy 306, 132463. https://doi.org/10.1016/j.energy.2024.132463.

Chiang, W.S., Chen, J.H., Jacobi, D., Yildirim, T., Turkoglu, D., Althaus, S., Liu, Y., 2020. Structural properties of kerogens with different maturities. Energy Fuels 34 (10), 12354–12365. https://doi.org/10.1021/acs.energyfuels.0c02268.

Correia, L.P., de Santana, C.P., da Silva, K.M.A., Ramos Júnior, F.J.D.L., Lima, R.S.C., de Souza, F.S., de Medeiros, A.C.D., Macêdo, R.O., 2018. Physical and chemical characteristics of Maytenus rigida in different particle sizes using SEM/EDS, TG/DTA and pyrolysis GC–MS. J. Therm. Anal. Calorim. 131 (1), 743–752.

Craddock, P.R., Haecker, A., Bake, K.D., Pomerantz, A.E., 2020. Universal curves describing the chemical and physical evolution of type II kerogen during thermal maturation. Energy Fuels 34 (12), 15217–15233. https://doi.org/10.1021/acs.energyfuels.0c02376.

Curtis, J.B., 2002. Fractured shale-gas systems. AAPG (Am. Assoc. Pet. Geol.) Bull. 86 (11), 1921–1938. https://doi.org/10.1306/61EEDDBE-173E-11D7-8645000102C1865D.

Curtis, M.E., Cardott, B.J., Sondergeld, C.H., Rai, C.S., 2012. The development of organic porosity in the woodford shale related to thermal maturity. In: SPE Annual Technical Conference and Exhibition? SPE. https://doi.org/10.2118/160158-MS. SPE-160158.

Curtis, M.E., Sondergeld, C.H., Rai, C.S., 2013. Relationship between organic shale microstructure and hydrocarbon generation. In: SPE Unconventional Resources Conference/Gas Technology Symposium. SPE. https://doi.org/10.2118/164540-MS. SPE-164540.

Dai, S., Jiang, J., 1990. Geochemical characteristics of the shallow natural gas in Jianghan Basin and its origin. Petrol. Explor. Dev. (6), 13–20.

Dang, Y., Zhao, L., Lu, X., Xu, J., Sang, P., Guo, S., Zhu, H., Guo, W., 2017. Molecular simulation of CO2/CH4 adsorption in brown coal: effect of oxygen-, nitrogen-, and sulfur-containing functional groups. Appl. Surf. Sci. 423, 33–42. https://doi.org/10.1016/j.apsusc.2017.06.143.

Deng, E.D., Yi, T.S., Yan, Z.H., Jiang, B.R., Wang, R., Fu, W., 2020. Accumulation condition and shale gas potential of the marineterrestrial transitional facies: a case study of Jinshacan 1 well of Longtan formation in northern Guizhou. J. China Inst. Min. Technol. 49 (6), 1166–1181.

Ding, A., Wang, M., Li, B., Zhang, D., Peng, X., Hui, R., 2003. Biogas forming mechanism and geochemical characteristics of its source rock. Nat. Gas Geosci. 14 (5), 402–407. https://doi.org/10.11764/j.issn.1672-1926.2003.05.402.

Donadelli, J.A., Canneva, A., Erra, G., Calvo, A., 2019. XPS direct analysis on shale rocks: correlation with kerogen type and maturity. Fuel 257, 116004. https://doi.org/10.1016/j.fuel.2019.116004.

Dong, D., Wang, Y., Li, X., et al., 2016. Breakthrough and prospect of shale gas exploration and development in China. Nat. Gas. Ind. B 3 (1), 12–26. https://doi.org/10.1016/j.ngib.2016.02.002.

Dowey, P.J., Taylor, K.G., 2020. Diagenetic mineral development within the upper Jurassic Haynesville-Bossier shale, USA. Sedimentology 67 (1), 47–77. https://doi.org/10.1111/sed.12624.

El-Habaak, G., Khalaphallah, R., Hassan, M., Askalany, M., Abdel-Hakeem, M., 2020. Characterization and exploitation of black shale as unconventional source of biohydrogen: a case study from the Abu-Tartur mine, Western desert, Egypt. Arabian J. Geosci. 13 (12), 467.

Elkady, Y., Kovscek, A.R., 2020. Multiscale study of CO2 impact on fluid transport and carbonate dissolution in Utica and Eagle Ford shale. J. Petrol. Sci. Eng. 195, 107867. https://doi.org/10.1016/j.petrol.2020.107867.

Faboya, O.L., Sonibare, O.O., Xu, J., Olowookere, N., Liao, Z., 2020. Mineralogical and pore structure of organic-rich deltaic shales and sub-bituminous coals from early Maastrichtian Mamu formation, Anambra Basin, Nigeria. SN Appl. Sci. 2 (12), 2057.

Fan, B., Shi, L., Wang, X., Wang, C., Li, Y., Huang, F., 2022. The distribution of gas components within a shale system and its implication for migration. Minerals 12 (4), 397. https://doi.org/10.3390/min12040397.

Fang, C., Xiong, Y., Liang, Q., Li, Y., 2012. Variation in abundance and distribution of diamondoids during oil cracking. Org. Geochem. 47, 1–8. https://doi.org/10.1016/j.orggeochem.2012.03.003.

Fleury, M., Gimmi, T., Mazurek, M., 2022. Porewater content, pore structure and water mobility in clays and shales from NMR methods. Clays Clay Miner. 70 (3), 417–437.
Fookes, C.J., Duffy, G.J., Udaja, P., Chensee, M.D., 1990. Mechanisms of thermal alteration of shale oils. Fuel 69 (9), 1142–1144. https://doi.org/10.1016/0016-2361(90)90071-W.
Fu, H., Wang, X., Zhang, L., Gao, R., Li, Z., Xu, T., Zhu, X., Xu, W., Li, Q., 2015. Investigation of the factors that control the development of pore structure in lacustrine shale: a case study of block X in the ordos Basin, China. J. Nat. Gas Sci. Eng. 26, 1422–1432. https://doi.org/10.1016/j.jngse.2015.07.025.
Fu, J., Wei, X., Luo, S., Zuo, Z., Zhou, H., Liu, B., Kong, Q., Zhan, S., Nan, J., 2019. Discovery and geological knowledge of the large deep coal-formed Qingyang Gas Field, Ordos Basin, NW China. Petrol. Explor. Dev. 46 (6), 1111–1126. https://doi.org/10.1016/S1876-3804(19)60267-3.
Furmann, A., Mastalerz, M., Schimmelmann, A., Pedersen, P.K., Bish, D., 2014. Relationships between porosity, organic matter, and mineral matter in mature organic-rich marine mudstones of the belle fourche and second white specks formations in Alberta, Canada. Mar. Petrol. Geol. 54, 65–81. https://doi.org/10.1016/j.marpetgeo.2014.02.020.
Gajica, G., Šajnović, A., Stojanović, K., Schwarzbauer, J., Kostić, A., Jovančićević, B., 2022. A comparative study of the molecular and isotopic composition of biomarkers in immature oil shale (aleksinac deposit, Serbia) and its liquid pyrolysis products (open and closed systems). Mar. Petrol. Geol. 136, 105383. https://doi.org/10.1016/j.marpetgeo.2021.105383.
Gao, J., Liu, G., Yang, W., Zhao, D., Chen, W., Liu, L., 2016. Geological and geochemical characterization of lacustrine shale, a case study of Lower Jurassic Badaowan shale in the Junggar Basin, Northwest China. J. Nat. Gas Sci. Eng. 31, 15–27. https://doi.org/10.1016/j.jngse.2016.03.006.
Gao, Y., Li, T., Guan, X., Niu, H., Kong, X., 2018. Mass method adsorption characteristics of shale gas under high pressure. Petroleum Geology & Experiment 40 (4), 566–572. https://doi.org/10.11781/sysydz201804566.
Gao, Z., Fan, Y., Xuan, Q., Zheng, G., 2020. A review of shale pore structure evolution characteristics with increasing thermal maturities. Advances in Geo-Energy Research 4 (3), 247–259.
Gasparik, M., Ghanizadeh, A., Bertier, P., Gensterblum, Y., Bouw, S., Krooss, B.M., 2012. High-pressure methane sorption isotherms of black shales from the Netherlands. Energy Fuels 26 (8), 4995–5004. https://doi.org/10.1021/ef300405g.
Ghanizadeh, A., Clarkson, C.R., Clarke, K.M., et al., 2020. Effects of entrained hydrocarbon and organic-matter components on reservoir quality of organic-rich shales: implications for “sweet spot” identification and enhanced-oil-recovery applications in the Duvernay Formation (Canada). SPE J. 25 (3), 1351–1376. https://doi.org/10.2118/189787-PA.
Ghosh Dastidar, S., Sarkar, K., Chandra, D., Hazra, B., Vishal, V., 2025. Investigating pore characteristics and their dependence on shale composition: case study from a Permian basin in India. ACS Omega 10 (5), 4395–4405. https://doi.org/10.1021/acsomega.4c07214.
Glorioso, J.C., Rattia, A., 2012. Unconventional reservoirs: basic petrophysical concepts for shale gas. In: SPE/EAGE European Unconventional Resources Conference and Exhibition. SPE. https://doi.org/10.2118/153004-MS. SPE-153004.
Gonciaruk, A., Hall, M.R., Fay, M.W., Parmenter, C.D., Vane, C.H., Khlobystov, A.N., Ripepi, N., 2021. Kerogen nanoscale structure and CO2 adsorption in shale micropores. Sci. Rep. 11 (1), 3920.
Goodarzi, F., Fowler, M.G., Bustin, M., McKirdy, D.M., 1992. Thermal maturity of early Paleozoic sediments as determined by the optical properties of marine-derived organic matter—A review. Early Organic Evolution: Implications for Mineral and Energy Resources 279–295.
Guo, S., Peng, Y., 2019. Determination method of shale gas content: a case study in the Ordos Basin, China. J. Petrol. Sci. Eng. 173, 95–100. https://doi.org/10.1016/j.petrol.2018.10.013.
Guo, X., Shen, Y., He, S., 2015. Quantitative pore characterization and the relationship between pore distributions and organic matter in shale based on Nano-CT image analysis: a case study for a lacustrine shale reservoir in the Triassic Chang 7 member, Ordos Basin, China. J. Nat. Gas Sci. Eng. 27, 1630–1640. https://doi.org/10.1016/j.jngse.2015.10.033.
Guo, X., Qin, Z., Yang, R., Dong, T., He, S., Hao, F., Yi, J., Shu, Z., Bao, H., Liu, K., 2019. Comparison of pore systems of clay-rich and silica-rich gas shales in the lower Silurian longmaxi formation from the Jiaoshiba area in the eastern Sichuan Basin, China. Mar. Petrol. Geol. 101, 265–280. https://doi.org/10.1016/j.marpetgeo.2018.11.038.
Guo, C., Li, R., Sun, J., Wang, X., Liu, H., 2020. A review of gas transport and adsorption mechanisms in two-component methane-carbon dioxide system. Int. J. Energy Res. 44 (4), 2499–2516. https://doi.org/10.1002/er.5114.
Han, J., Sun, Y., Guo, W., Li, Q., Deng, S., 2019. Characterization of pyrolysis of Nong'an oil shale at different temperatures and analysis of pyrolysate. Oil Shale 36 (2S), 151–170. https://doi.org/10.3176/oil.2019.2S.06.
Hao, M., Qiao, Z., Zhang, H., Wang, Y., Li, Y., 2021. Thermodynamic analysis of CH4/CO2/N2 adsorption on anthracite coal: investigated by molecular simulation. Energy Fuels 35 (5), 4246–4257. https://doi.org/10.1021/acs.energyfuels.0c04337.
Harper, J.A., 2008. The Marcellus shale–An old “new” gas reservoir in Pennsylvania. Penn. Geol. 38 (1), 2–13.
Hazra, B., Vishal, V., Singh, D.P., 2020. Applicability of low-pressure CO2 and N2 adsorption in determining pore attributes of organic-rich shales and coals. Energy Fuels 35 (1), 456–464. https://doi.org/10.1021/acs.energyfuels.0c03412.
He, Z., Nie, H., Zhao, J., Liu, W., Bao, F., Zhang, W., 2017. Types and origin of nanoscale pores and fractures in Wufeng and Longmaxi shale in Sichuan Basin and its periphery. J. Nanosci. Nanotechnol. 17 (9), 6626–6633. https://doi.org/10.1166/jnn.2017.14425.
He, J., Li, X., Yin, C., Zhang, Y., Lin, C., 2020. Propagation and characterization of the micro cracks induced by hydraulic fracturing in shale. Energy 191, 116449. https://doi.org/10.1016/j.energy.2019.116449.
Heald, M.T., 1950. Authigenesis in West Virginia sandstones. J. Geol. 58 (6), 624–633. https://doi.org/10.1086/625773.
Higgs, K.E., Zwingmann, H., Reyes, A.G., Funnell, R.H., 2007. Diagenesis, porosity evolution, and petroleum emplacement in tight gas reservoirs, Taranaki Basin, New Zealand. J. Sediment. Res. 77 (12), 1003–1025. https://doi.org/10.2110/jsr.2007.095.
Horsfield, B., Zou, C., Li, J., Yang, S., Mahlstedt, N., Misch, D., Gross, D., Wei, M., Wang, Y., Tan, J., 2021. Prediction of the gas-generating characteristics of the Qiongzhusi and Longmaxi Formations, Yangtze Platform, Southern China, using analogues. AAPG (Am. Assoc. Pet. Geol.) Bull. 105 (5), 945–985. https://doi.org/10.1306/11182018244.
Hou, H., Yang, W., Yang, R., Jiang, Z., Miao, K., Sun, W., Xiao, Y., 2025. Formation and evolution of complex pore-fracture systems in shale gas reservoirs: Insights into controlling mechanisms. Energy Fuels 39 (6), 3008–3038. https://doi.org/10.1021/acs.energyfuels.4c05306.
Hu, H., Zhang, T., Wiggins-Camacho, J.D., Ellis, G.S., Lewan, M.D., Zhang, X., 2015. Experimental investigation of changes in methane adsorption of bitumen-free Woodford Shale with thermal maturation induced by hydrous pyrolysis. Mar. Petrol. Geol. 59, 114–128. https://doi.org/10.1016/j.marpetgeo.2014.07.029.
Hu, G., Pang, Q., Jiao, K., Hu, C., Liao, Z., 2020a. Development of organic pores in the Longmaxi Formation overmature shales: Combined effects of thermal maturity and organic matter composition. Mar. Petrol. Geol. 116, 104314. https://doi.org/10.1016/j.marpetgeo.2020.104314.
Hu, Y., Wang, S., He, Y., 2020b. Investigation of the coal oxidation effect on competitive adsorption characteristics of $CO_2$/$CH_4$. Energy Fuels 34 (10), 12860–12869. https://doi.org/10.1021/acs.energyfuels.0c02497.
Huang, H., Huang, B., Huang, Y., Li, X., Tian, H., 2017. Condensate origin and hydrocarbon accumulation mechanism of the deepwater giant gas field in western South China Sea: A case study of Lingshui 17-2 gas field in Qiongdongnan Basin. Petrol. Explor. Dev. 44 (3), 409–417. https://doi.org/10.1016/S1876-3804(17)30047-2.
Huang, L., Ning, Z., Wang, Q., Zhang, W., Cheng, Z., Wu, X., Qin, H., 2018. Effect of organic type and moisture on $CO_2$/$CH_4$ competitive adsorption in kerogen with implications for $CO_2$ sequestration and enhanced $CH_4$ recovery. Appl. Energy 210, 28–43. https://doi.org/10.1016/j.apenergy.2017.10.122.
Hunt, J.M., 1991. Generation of gas and oil from coal and other terrestrial organic matter. Org. Geochem. 17 (6), 673–680. https://doi.org/10.1016/0146-6380(91)90011-8.
Iqbal, O., Padmanabhan, E., Mandal, A., Dvorkin, J., 2021. Characterization of geochemical properties and factors controlling the pore structure development of shale gas reservoirs. J. Petrol. Sci. Eng. 206, 109001. https://doi.org/10.1016/j.petrol.2021.109001.
Jarvie, D.M., Hill, R.J., Ruble, T.E., Pollastro, R.M., 2007. Unconventional shale-gas systems: the Mississippian Barnett Shale of north-central Texas as one model for thermogenic shale-gas assessment. AAPG (Am. Assoc. Pet. Geol.) Bull. 91 (4), 475–499. https://doi.org/10.1306/12190606068.
Jiao, F., 2019. Theoretical insights, core technologies and practices concerning “volume development” of shale gas in China. Nat. Gas. Ind. B 6 (6), 525–538. https://doi.org/10.1016/j.ngib.2019.05.001.
Jin, Z., Nie, H., Liu, Q., Zhao, J., Jiang, T., 2018. Source and seal coupling mechanism for shale gas enrichment in upper Ordovician Wufeng Formation-Lower Silurian Longmaxi Formation in Sichuan Basin and its periphery. Mar. Petrol. Geol. 97, 78–93. https://doi.org/10.1016/j.marpetgeo.2018.06.009.
Jin, Z., Zhu, R., Shen, Y., 2021. Several issues worthy of attention in current lacustrine shale oil exploration and development. Petrol. Explor. Dev. 48 (6), 1471–1484. https://doi.org/10.1016/S1876-3804(21)60303-8.
Jochum, J., 2000. Variscan and Post-Variscan lead–zinc mineralization, Rhenish Massif, Germany: evidence for sulfide precipitation via thermochemical sulfate reduction. Miner. Deposita 35 (5), 451–464.
Ju, Y., Wang, G., Bu, H., Li, Q., Yan, Z., 2014. China organic-rich shale geologic features and special shale gas production issues. J. Rock Mech. Geotech. Eng. 6 (3), 196–207. https://doi.org/10.1016/j.jrmge.2014.03.002.
Kang, Z., Zhao, Y., Yang, D., 2020. Review of oil shale in-situ conversion technology. Appl. Energy 269, 115121. https://doi.org/10.1016/j.apenergy.2020.115121.
Khatibi, S., Ostadhassan, M., Tuschel, D., Gentzis, T., Carvajal-Ortiz, H., 2018. Evaluating molecular evolution of kerogen by raman spectroscopy: Correlation with optical microscopy and rock-eval pyrolysis. Energies 11 (6), 1406. https://doi.org/10.3390/en11061406.
Kim, J., Kim, D., Lee, W., Lee, Y., Kim, H., 2017. Impact of total organic carbon and specific surface area on the adsorption capacity in Horn River shale. J. Petrol. Sci. Eng. 149, 331–339. https://doi.org/10.1016/j.petrol.2016.10.053.
King, G.R., 1993. Material-balance techniques for coal-seam and devonian shale gas reservoirs with limited water influx. SPE Reserv. Eng. 8 (1), 67–72. https://doi.org/10.2118/20730-PA.
Klaver, J., Desbois, G., Littke, R., Urai, J.L., 2015. BIB-SEM characterization of pore space morphology and distribution in postmature to overmature samples from the Haynesville and Bossier Shales. Mar. Petrol. Geol. 59, 451–466. https://doi.org/10.1016/j.marpetgeo.2014.09.020.

Kuang, L.C., Hou, L.H., Wu, S.T., Cui, J.W., Tian, H., Zhang, L.J., Zhao, Z.Y., Luo, X., Jiang, X.H., 2022. Organic matter occurrence and pore-forming mechanisms in lacustrine shales in China. Pet. Sci. 19 (4), 1460–1472. https://doi.org/10.1016/j.petsci.2022.03.005.

Lai, J., Wang, G.W., Meng, C.Q., Guan, B., Zheng, X.H., Zhou, L., Xin, Y., Han, C., 2015. Pore structure characteristics and formation mechanisms analysis of tight gas sandstones. Prog. Geophys. 30 (1), 217–227. https://doi.org/10.6038/pg20150133.

Li, Y., Jiang, Z., Liang, S., Zhu, J., Huang, Y., Luan, T., 2016. Hydrocarbon generation in the lacustrine mudstones of the Wenchang Formation in the Baiyun Sag of the Pearl River Mouth Basin, northern South China Sea. Energy Fuels 30 (1), 626–637. https://doi.org/10.1021/acs.energyfuels.5b02034.

Li, A., Ding, W., Zhou, X., Cao, X., Zhang, M., Fu, F., Chen, E., 2017. Investigation of the methane adsorption characteristics of marine shale: A case study of Lower Cambrian Qiongzhusi Shale in eastern Yunnan Province, South China. Energy Fuels 31 (3), 2625–2635. https://doi.org/10.1021/acs.energyfuels.6b03168.

Li, J., Zhou, S., Gaus, G., Li, Y., Ma, Y., Chen, K., Zhang, Y., 2018. Characterization of methane adsorption on shale and isolated kerogen from the Sichuan Basin under pressure up to 60 MPa: Experimental results and geological implications. Int. J. Coal Geol. 189, 83–93. https://doi.org/10.1016/j.coal.2018.02.020.

Li, W., Pang, X., Snape, C., Zhang, B., Zheng, D., Zhang, X., 2019a. Molecular simulation study on methane adsorption capacity and mechanism in clay minerals: Effect of clay type, pressure, and water saturation in shales. Energy Fuels 33 (2), 765–778. https://doi.org/10.1021/acs.energyfuels.8b03462.

Li, Y., Wang, Z., Pan, Z., Niu, X., Yu, Y., Meng, S., 2019b. Pore structure and its fractal dimensions of transitional shale: A cross-section from east margin of the Ordos Basin, China. Fuel 241, 417–431. https://doi.org/10.1016/j.fuel.2018.12.066.

Li, Z., Jiang, Z., Yu, H., Liang, Z., 2019c. Organic matter pore characterization of the Wufeng-Longmaxi shales from the fuling gas field, Sichuan Basin: evidence from organic matter isolation and low-pressure $CO_2$ and $N_2$ adsorption. Energies 12 (7), 1207. https://doi.org/10.3390/en12071207.

Li, X., Jiang, Z., Jiang, S., Li, Z., Song, Y., Jiang, H., Qiu, H., Cao, X., Miao, Y., 2020a. Various controlling factors of matrix-related pores from differing depositional shales of the Yangtze Block in South China: Insight from organic matter isolation and fractal analysis. Mar. Petrol. Geol. 111, 720–734. https://doi.org/10.1016/j.marpetgeo.2019.08.019.

Li, Y., Li, M., Zhang, J., Pang, Q., Zou, C., Shu, H., Wang, G., 2020b. Influence of the Emeishan basalt eruption on shale gas enrichment: A case study of shale from Wufeng-Longmaxi formations in northern Yunnan and Guizhou provinces. Fuel 282, 118835. https://doi.org/10.1016/j.fuel.2020.118835.

Li, Y., Chen, S., Lu, J., Wang, G., Zou, X., Xiao, Z., Su, K., He, Q., Luo, X., 2020c. The logging recognition of solid bitumen and its effect on physical properties, AC, resistivity and NMR parameters. Mar. Petrol. Geol. 112, 104070. https://doi.org/10.1016/j.marpetgeo.2019.104070.

Li, Y., Chen, S., Liu, X., Wu, B., Zhang, J., He, X., Mou, F., Luo, L., 2022. Study on the logging response characteristics and the quantitative identification method of solid bitumen at different thermal evolution stages. Fuel 316, 123424. https://doi.org/10.1016/j.fuel.2022.123424.

Liang, F., 1985. Characteristics of hydrocarbons from Huanghua Depression. Acta Pet. Sin. 6 (1), 17–23.

Liang, L., Xiong, J., Liu, X., 2015. An investigation of the fractal characteristics of the Upper Ordovician Wufeng Formation shale using nitrogen adsorption analysis. J. Nat. Gas Sci. Eng. 27, 402–409. https://doi.org/10.1016/j.jngse.2015.07.023.

Lis, G.P., Topor, T., Mastalerz, M., 2025. Organic matter content and its role in shale porosity development with maturity: Insights from Baltic Basin Silurian shales. Int. J. Coal Geol. 301, 104713. https://doi.org/10.1016/j.coal.2025.104713.

Liu, L., 2020. Characteristics of Structure Evolution and Pore Development of Organic Matter in Shale of Wufeng-Longmaxi Formation, Northern Guizhou. China University of Geosciences, Beijing. https://doi.org/10.27493/d.cnki.gzdzy.2020.000330.

Liu, X., Dong, Q., Dong, Q., Pan, J., Ding, W., Zhang, Y., Sun, X., 2013a. Characteristics of methane isothermal adsorption for Paleozoic shale in Subei Area. Geoscience 27 (5), 1219–1224.

Liu, D., Xiao, X., Tian, H., Min, Y., Zhou, Q., Cheng, P., Shen, J., 2013b. Sample maturation calculated using Raman spectroscopic parameters for solid organics: Methodology and geological applications. Chin. Sci. Bull. 58 (11), 1285–1298.

Liu, H., Zhang, S., Song, G., Zhang, S., Hao, X., Xie, Z., Xu, N., Liu, P., 2017a. A discussion on the origin of shale reservoir inter-laminar fractures in the Shahejie Formation of Paleogene, Dongying Depression. J. Earth Sci. 28 (6), 1064–1077.

Liu, R., Liu, Z., Sun, P., Yang, X., Zhang, C., 2017b. Shale gas accumulation potential of the Upper Cretaceous Qingshankou Formation in the southeast Songliao Basin, NE China. Mar. Petrol. Geol. 86, 547–562. https://doi.org/10.1016/j.marpetgeo.2017.05.014.

Liu, Y., Zhu, Y., Liu, S., Li, W., Tang, X., 2018. Temperature effect on gas adsorption capacity in different sized pores of coal: Experiment and numerical modeling. J. Petrol. Sci. Eng. 165, 821–830. https://doi.org/10.1016/j.petrol.2018.03.021.

Liu, Z., Chen, D., Zhang, J., Lü, X., Wang, Z., Liao, W., Shi, X., Tang, J., Xie, G., 2019a. Pyrite morphology as an indicator of paleoredox conditions and shale gas content of the Longmaxi and Wufeng shales in the middle Yangtze area, South China. Minerals 9 (7), 428. https://doi.org/10.3390/min9070428.

Liu, K., Wang, L., Ostadhassan, M., Zou, J., Bubach, B., Rezaee, R., 2019b. Nanopore structure comparison between shale oil and shale gas: Examples from the Bakken and Longmaxi Formations. Pet. Sci. 16 (1), 77–93.

Liu, X., Lai, J., Fan, X., Shu, H., Wang, G., Ma, X., Liu, M., Guan, M., Luo, Y., 2020. Insights in the pore structure, fluid mobility and oiliness in oil shales of Paleogene Funing Formation in Subei Basin, China. Mar. Petrol. Geol. 114, 104228. https://doi.org/10.1016/j.marpetgeo.2020.104228.

Liu, W., Xu, Q., Wang, H., Liu, P., Guo, R., Zhang, Y., Wei, K., 2022a. Quantitative characterization of pore network and influencing factors of methane adsorption capacity of transitional shale from the southern North China Basin. J. Pet. Explor. Prod. Technol. 12 (3), 793–810.

Liu, B., Mastalerz, M., Schieber, J., 2022b. SEM petrography of dispersed organic matter in black shales: A review. Earth Sci. Rev. 224, 103874. https://doi.org/10.1016/j.earscirev.2021.103874.

Löhr, S.C., Baruch, E.T., Hall, P.A., Kennedy, M.J., 2015. Is organic pore development in gas shales influenced by the primary porosity and structure of thermally immature organic matter? Org. Geochem. 87, 119–132. https://doi.org/10.1016/j.orggeochem.2015.07.010.

Long, S., Feng, D., Li, F., Du, W., 2018. Prospect analysis of the deep marine shale gas exploration and development in the Sichuan Basin, China. Journal of Natural Gas Geoscience 3 (4), 181–189. https://doi.org/10.1016/j.jnggs.2018.11.001.

Loucks, R.G., Reed, R.M., 2015. Distinguishing organic matter pores associated with depositional organic matter versus migrated organic matter in mudrocks. In: AAPG Annual Convention and Exhibition.

Loucks, R.G., Reed, R.M., Ruppel, S.C., Jarvie, D.M., 2009. Morphology, genesis, and distribution of nanometer-scale pores in siliceous mudstones of the Mississippian Barnett Shale. J. Sediment. Res. 79 (12), 848–861. https://doi.org/10.2110/jsr.2009.092.

Loucks, R.G., Reed, R.M., Ruppel, S.C., Hammes, U., 2012. Spectrum of pore types and networks in mudrocks and a descriptive classification for matrix-related mudrock pores. AAPG (Am. Assoc. Pet. Geol.) Bull. 96 (6), 1071–1098. https://doi.org/10.1306/08171111061.

Lu, L., Liu, W., Wei, Z., Pan, A., Zhang, Q., Teng, G., 2022. Diagenesis of the Silurian Shale, Sichuan Basin: Focus on pore development and preservation. Acta Sedimentol. Sin. 40 (1), 73–87. https://doi.org/10.14027/j.issn.1000-0550.2021.125.

Lu, M., Duan, G., Zhang, T., Liu, N., Song, Y., Zhang, Z., Qiao, J., Wang, Z., Fang, Z., Luo, Q., 2025. Influences of paleoclimatic changes on organic matter enrichment mechanisms in freshwater and saline lacustrine oil shales in China: A machine learning approach. Earth Sci. Rev., 105061 https://doi.org/10.1016/j.earscirev.2025.105061.

Luo, P., Zhong, N., 2020. The role of residual bitumen on the pore structure of organic-rich shales from low to over mature: Insight from shale and coal samples after the hydrous pyrolysis. Int. J. Coal Geol. 226, 103515. https://doi.org/10.1016/j.coal.2020.103515.

Luo, X., Jin, Z., Liu, K., Zhang, S., 2017. Geofluids in deep sedimentary basins and their significance for petroleum accumulation. Geofluids (2), 1–4. https://doi.org/10.1155/2017/3571359.

Luo, P., Zhong, N., Khan, I., Wang, X., Wang, H., Luo, Q., Guo, Z., 2019. Effects of pore structure and wettability on methane adsorption capacity of mud rock: Insights from mixture of organic matter and clay minerals. Fuel 251, 551–561. https://doi.org/10.1016/j.fuel.2019.04.072.

Luo, Q., Zhang, L., Zhong, N., et al., 2021. Thermal evolution behavior of the organic matter and a ray of light on the origin of vitrinite-like maceral in the Mesoproterozoic and Lower Cambrian black shales: Insights from artificial maturation. Int. J. Coal Geol. 244, 103813. https://doi.org/10.1016/j.coal.2021.103813.

Luo, Q., Goodarzi, F., Zhong, N., et al., 2025. Dispersed organic matter from Pre-Devonian marine shales: A review on its composition, origin, evolution, and potential for hydrocarbon prospecting. Earth Sci. Rev. 261, 105027. https://doi.org/10.1016/j.earscirev.2024.105027.

Ma, X., 2019. Enrichment laws and scale effective development of shale gas in the southern Sichuan Basin. Nat. Gas. Ind. B 6 (3), 240–249. https://doi.org/10.1016/j.ngib.2018.10.005.

Ma, X., Guo, S., 2021. Study on pore evolution and diagenesis division of a Permian Longtan transitional shale in Southwest Guizhou, China. Energy Sci. Eng. 9 (1), 58–79. https://doi.org/10.1002/ese3.813.

Ma, Y., Zhong, N., Li, D., Pan, Z., Cheng, L., Liu, K., 2015. Organic matter/clay mineral intergranular pores in the Lower Cambrian Lujiaping Shale in the northeastern part of the upper Yangtze Area, China: A possible microscopic mechanism for gas preservation. Int. J. Coal Geol. 137, 38–54. https://doi.org/10.1016/j.coal.2014.11.001.

Ma, Z., Zheng, L., Xu, X., Bao, F., Yu, X., 2017a. Thermal simulation experiment on the formation and evolution of organic pores in organic-rich shale. Acta Pet. Sin. 38 (1), 23. https://doi.org/10.7623/syxb201701003.

Ma, Z., Zheng, L., Xu, X., Bao, F., Yu, X., 2017b. Thermal simulation experiment of organic matter-rich shale and implication for organic pore formation and evolution. Petroleum Research 2 (4), 347–354. https://doi.org/10.1016/j.ptlrs.2017.04.005.

Ma, H., Peng, Q., An, Z., Huang, W., Shuai, Z., 2018. Efficient and long-lived room-temperature organic phosphorescence: Theoretical descriptors for molecular designs. J. Am. Chem. Soc. 141 (2), 1010–1015. https://doi.org/10.1021/jacs.8b11224.

MacGowan, D.B., Jiao, Z.S., Surdam, R.C., Miknis, F.P., 1993. Normally pressured Vs. Abnormally pressured compartments in sandstones in the Powder River Basin, Wyoming: A comparative study of the muddy sandstone and the Minnelusa Formation, pp. 281–295.

Makeen, Y.M., Hakimi, M.H., Abdullah, W.H., Mustapha, K.A., Hassan, M.H.A., Shushan, I.E., Garba, T.E., Abujaish, Y.A., Lashin, A.A., 2020. Basin modelling and

bulk kinetics of heterogeneous organic-rich Nyalau Formation sediments of the Sarawak Basin, Malaysia. J. Petrol. Sci. Eng. 195, 107595. https://doi.org/10.1016/j.petrol.2020.107595.
Mani, D., Kalpana, M.S., Patil, D.J., Dayal, A.M., 2017. Organic matter in gas shales: Origin, evolution, and characterization. In: Shale Gas 25-54. https://doi.org/10.1016/B978-0-12-809573-7.00003-2.
Mastalerz, M., Schieber, J., 2017. Effect of ion milling on the perceived maturity of shale samples: implications for organic petrography and SEM analysis. Int. J. Coal Geol. 183, 110–119. https://doi.org/10.1016/j.coal.2017.10.010.
Mazumder, M., Bal, A., Tripathy, A., Liu, S., Singh, T.N., 2024. Multiscale assessment of transformation in pore System of shale during combustion: An Insight into poromechanical response and sorption dynamics. Energy Fuels 38 (18), 17510–17524. https://doi.org/10.1021/acs.energyfuels.4c02383.
Miao, Y., Li, X., Wang, X., Chen, Y., Zhou, Y., Liu, F., Xia, J., 2017. Review on hydrocarbon generation, pores formation and its methane adsorption mechanism in shale kerogen. Scientia Sinica Physica, Mechanica & Astronomica 47 (11), 114604. https://doi.org/10.1360/SSPMA2016-00539.
Milliken, K.L., Rudnicki, M., Awwiller, D.N., Zhang, T., 2013. Organic matter–hosted pore system, Marcellus Formation (Devonian), Pennsylvania. AAPG (Am. Assoc. Pet. Geol.) Bull. 97 (2), 177–200. https://doi.org/10.1306/07231212048.
Misch, D., Mendez-Martin, F., Hawranek, G., Onuk, P., Groß, D., Sachsenhofer, R.F., 2016. SEM and FIB-SEM investigations on potential gas shales in the Dniepr-Donets Basin (Ukraine): Pore space evolution in organic matter during thermal maturation. IOP Conf. Ser. Mater. Sci. Eng. 109 (1), 012010. https://doi.org/10.1088/1757-899X/109/1/012010. IOP Publishing.
Mishra, D.K., Varma, A.K., Mendhe, V.A., Agrawal, S., Singh, B.D., Hackley, P.C., 2021. Organo-facies and mineral effects on sorption capacity of low-maturity Permian Barakar shales from the Auranga Basin, Jharkhand, India. Energy Fuels 35 (9), 7717–7737. https://doi.org/10.1021/acs.energyfuels.0c04310.
Miskolczi, N., Nagy, R., 2012. Hydrocarbons obtained by waste plastic pyrolysis: comparative analysis of decomposition described by different kinetic models. Fuel Process. Technol. 104, 96–104. https://doi.org/10.1016/j.fuproc.2012.04.031.
Montgomery, S.L., Jarvie, D.M., Bowker, K.A., Pollastro, R.M., 2005. Mississippian Barnett Shale, Fort Worth basin, north-central Texas: Gas-shale play with multi–trillion cubic foot potential. AAPG (Am. Assoc. Pet. Geol.) Bull. 89 (2), 155–175. https://doi.org/10.1306/09170404042.
Nie, H., Jin, Z., Sun, C., He, Z., Liu, G., Liu, Q., 2019a. Organic matter types of the Wufeng and Longmaxi Formations in the Sichuan Basin, South China: Implications for the formation of organic matter pores. Energy Fuels 33 (9), 8076–8100. https://doi.org/10.1021/acs.energyfuels.9b01453.
Nie, H., Sun, C., Liu, G., Du, W., He, Z., 2019b. Dissolution pore types of the Wufeng Formation and the Longmaxi Formation in the Sichuan Basin, South China: Implications for shale gas enrichment. Mar. Petrol. Geol. 101, 243–251. https://doi.org/10.1016/j.marpetgeo.2018.11.042.
Nie, H., He, Z., Liu, G., Du, W., Wang, R., Zhang, G., 2021. Genetic mechanism of high-quality shale gas reservoirs in the Wufeng–LongmaxiFms in the Sichuan Basin. Nat. Gas. Ind. B 8 (1), 24–34. https://doi.org/10.1016/j.ngib.2020.06.002.
Pang, X., Jia, C., Zhang, K., Li, M., Wang, Y., Peng, J., Li, B., Chen, J., 2020. The dead line for oil and gas and implication for fossil resource prediction. Earth Syst. Sci. Data 12 (1), 577–590. https://doi.org/10.5194/essd-12-577-2020.
Park, S.Y., Lee, H.S., Kim, S., Jeon, H.S., Choi, J., Han, Y., 2021. Correlation between adsorbed methane concentration and pore structure of organic-rich black shale from the Liard Basin, Canada. J. Nat. Gas Sci. Eng. 95, 104226. https://doi.org/10.1016/j.jngse.2021.104226.
Passey, Q.R., Bohacs, K.M., Esch, W.L., Klimentidis, R., Sinha, S., 2010. From oil-prone source rock to gas-producing shale reservoir–geologic and petrophysical characterization of unconventional shale-gas reservoirs. In: SPE International Oil and Gas Conference and Exhibition in China. SPE. https://doi.org/10.2118/131350-MS. SPE-131350.
Peng, W., Liu, Q., Hu, G., Lyu, Y., Zhu, D., Meng, Q., Guo, F., Wang, R., 2020. Mechanisms of carbon isotopic fractionation in the process of natural gas generation: Geochemical evidence from thermal simulation experiment. Petrol. Explor. Dev. 47 (5), 1042–1054. https://doi.org/10.1016/S1876-3804(20)60115-X.
Peters, K.E., 1986. Guidelines for evaluating petroleum source rock using programmed pyrolysis. AAPG (Am. Assoc. Pet. Geol.) Bull. 70 (3), 318–329. https://doi.org/10.1306/94885688-1704-11D7-8645000102C1865D.
Psarras, P., Holmes, R., Vishal, V., Wilcox, J., 2017. Methane and CO2 adsorption capacities of kerogen in the Eagle Ford shale from molecular simulation. Accounts Chem. Res. 50 (8), 1818–1828. https://doi.org/10.1021/acs.accounts.7b00003.
Qiao, J., Littke, R., Zieger, L., Jiang, Z., Fink, R., 2020. Controls on gas storage characteristics of Upper Paleozoic shales from the southeastern Ordos Basin. Mar. Petrol. Geol. 117, 104377. https://doi.org/10.1016/j.marpetgeo.2020.104377.
Qiu, Z., Song, D., Zhang, L., Zhang, Q., Zhao, Q., Wang, Y., Liu, H., Liu, D., Li, S., Li, X., 2021. The geochemical and pore characteristics of a typical marine–continental transitional gas shale: a case study of the permian Shanxi Formation on the eastern margin of the Ordos Basin. Energy Rep. 7, 3726–3736. https://doi.org/10.1016/j.egyr.2021.06.056.
Qu, Y., Chu, M., Hao, C., Zhang, C., Bai, S., 2017. Characteristics of oil shale particles fragmentation/pulverization during thermal effect. CIE J. 68 (10), 3934–3942. https://doi.org/10.13225/j.cnki.jccs.2017.1126.
Rexer, T.F., Benham, M.J., Aplin, A.C., Thomas, K.M., 2013. Methane adsorption on shale under simulated geological temperature and pressure conditions. Energy Fuels 27 (6), 3099–3109. https://doi.org/10.1021/ef400381v.
Rexer, T.F., Mathia, E.J., Aplin, A.C., Thomas, K.M., 2014. High-pressure methane adsorption and characterization of pores in Posidonia shales and isolated kerogens. Energy Fuels 28 (5), 2886–2901. https://doi.org/10.1021/ef402466m.
Rice, D.D., Claypool, G.E., 1981. Generation, accumulation, and resource potential of biogenic gas. AAPG (Am. Assoc. Pet. Geol.) Bull. 65 (1), 5–25. https://doi.org/10.1306/2F919765-16CE-11D7-8645000102C1865D.
Rodriguez, N.D., Philp, R.P., 2010. Geochemical characterization of gases from the Mississippian Barnett shale, Fort Worth basin, Texas. AAPG (Am. Assoc. Pet. Geol.) Bull. 94 (11), 1641–1656. https://doi.org/10.1306/04061009119.
Rohrback, B.G., Peters, K.E., Kaplan, I.R., 1984. Geochemistry of artificially heated humic and sapropelic sediments—Ii: oil and gas generation. AAPG (Am. Assoc. Pet. Geol.) Bull. 68 (8), 961–970. https://doi.org/10.1306/AD4616A1-16F7-11D7-8645000102C1865D.
Rojas, L.M., Silveira, L.S., Miranda, F., Corrêa, J.R., 2024. A novel approach to estimate TOC in unconventional reservoirs: the case of the Pimenteiras shale, Parnaíba Basin, Brazil. In: SPWLA Annual Logging Symposium. SPWLA, D051S017R005. https://doi.org/10.30632/SPWLA-2024-0101.
Romero-Sarmiento, M.F., Ducros, M., Carpentier, B., Lorant, F., Cacas, M.C., Pegaz-Fiornet, S., Wolf, S., Rohais, S., Moretti, I., 2013. Quantitative evaluation of TOC, organic porosity and gas retention distribution in a gas shale play using petroleum system modeling: application to the Mississippian Barnett Shale. Mar. Petrol. Geol. 45, 315–330. https://doi.org/10.1016/j.marpetgeo.2013.04.003.
Ross, D.J., Bustin, R.M., 2009. The importance of shale composition and pore structure upon gas storage potential of shale gas reservoirs. Mar. Petrol. Geol. 26 (6), 916–927. https://doi.org/10.1016/j.marpetgeo.2008.06.004.
Rouquerol, J., Avnir, D., Fairbridge, C.W., Everett, D.H., Haynes, J.M., Pernicone, N., Ramsay, J.D.F., Sing, K.S.W., Unger, K.K., 1994. Recommendations for the characterization of porous solids (Technical Report). Pure Appl. Chem. 66 (8), 1739–1758.
Salygin, V., Guliev, I., Chernysheva, N., Sokolova, E., Toropova, N., Egorova, L., 2019. Global shale revolution: successes, challenges, and prospects. Sustainability 11 (6), 1627. https://doi.org/10.3390/su11061627.
Setzmann, U., Wagner, W., 1991. A new equation of state and tables of thermodynamic properties for methane covering the range from the melting line to 625 K at pressures up to 1000 MPa. J. Phys. Chem. Ref. Data 20 (6), 1061–1155. https://doi.org/10.1063/1.555898.
Shalaby, M.R., Hakimi, M.H., Abdullah, W.H., 2014. Diagenesis in the middle Jurassic Khatatba formation sandstones in the Shoushan Basin, northern Western Desert, Egypt. Geol. J. 49 (3), 239–255. https://doi.org/10.1002/gj.2512.
Shan, C., Zhang, T., Guo, J., Lang, X., Zhang, C., 2015. Geological characteristics and resource potential of the Upper Sinian Doushantuo Formation shale gas in the north of middle Yangtze region. Geology in China 42 (6), 1944.
Shao, D., Zhang, T., Ko, L.T., Li, Y., Yan, J., Zhang, L., Huo, H., Qiao, B., 2020. Experimental investigation of oil generation, retention, and expulsion within Type II kerogen-dominated marine shales: insights from gold-tube nonhydrous pyrolysis of Barnett and Woodford Shales using miniature core plugs. Int. J. Coal Geol. 217, 103337. https://doi.org/10.1016/j.coal.2019.103337.
Shao, L., Yang, Z., Fang, C., Wang, S., Gu, J., Zhang, W., Lu, J., 2021. Permo-Carboniferous marine-terrestrial transitional facies coal measures shale gas geological conditions and exploration potential in Qinshui Basin. Coal Geology of China 33 (10), 1–10.
Shi, M., Yu, B., Xue, Z., Wu, J., Yuan, Y., 2015. Pore characteristics of organic-rich shales with high thermal maturity: a case study of the Longmaxi gas shale reservoirs from well Yuye-1 in southeastern Chongqing, China. J. Nat. Gas Sci. Eng. 26, 948–959. https://doi.org/10.1016/j.jngse.2015.07.042.
Shi, M., Yu, B., Zhang, J., Huang, H., Yuan, Y., Li, B., 2018. Evolution of organic pores in marine shales undergoing thermocompression: a simulation experiment using hydrocarbon generation and expulsion. J. Nat. Gas Sci. Eng. 59, 406–413. https://doi.org/10.1016/j.jngse.2018.09.008.
Sircar, S., 1999. Gibbsian surface excess for gas adsorption revisited. Ind. Eng. Chem. Res. 38 (10), 3670–3682. https://doi.org/10.1021/ie9900871.
Slatt, R.M., O'Brien, N.R., 2011. Pore types in the Barnett and Woodford gas shales: contribution to understanding gas storage and migration pathways in fine-grained rocks. AAPG (Am. Assoc. Pet. Geol.) Bull. 95 (12), 2017–2030. https://doi.org/10.1306/03301110145.
Song, D., Tuo, J., Wu, C., Zhang, M., Su, L., 2020. Comparison of pore evolution for a Mesoproterozoic marine shale and a Triassic terrestrial mudstone during artificial maturation experiments. J. Nat. Gas Sci. Eng. 75, 103153. https://doi.org/10.1016/j.jngse.2020.103153.
Song, D., Wang, X., Tuo, J., Wu, C., Zhang, M., Su, L., He, W., 2021. A comprehensive study on the impacts of rock fabric on hydrocarbon generation and pore structure evolution of shale under semi-confined condition. Mar. Petrol. Geol. 124, 104830. https://doi.org/10.1016/j.marpetgeo.2020.10483.
Stevens, S.H., Moodhe, K.D., Kuuskraa, V.A., 2013. China shale gas and shale oil resource evaluation and technical challenges. In: SPE Asia Pacific Oil and Gas Conference and Exhibition. SPE. https://doi.org/10.2118/165832-MS. SPE-165832.
Su, J., Wang, X., Yang, H., Yu, F., Li, Y., Ma, S., Wei, C., Weng, N., Yang, Y., 2021. Hydrothermal alteration and hydrocarbon accumulations in ultra-deep carbonate reservoirs along a strike-slip fault system, Tarim Basin, NW China. J. Petrol. Sci. Eng. 203, 108605. https://doi.org/10.1016/j.petrol.2021.108605.
Suekuni, M.T., Craddock, P.R., Douglas, J.T., Pomerantz, A.E., Allgeier, A.M., 2022. Critical practices for the preparation and analysis of kerogen. Energy Fuels 36 (16), 8828–8843. https://doi.org/10.1021/acs.energyfuels.2c01063.

Suleimenova, A., Bake, K.D., Ozkan, A., Valenza II, J.J., Kleinberg, R.L., Burnham, A.K., Ferralis, N., Pomerantz, A.E., 2014. Acid demineralization with critical point drying: a method for kerogen isolation that preserves microstructure. Fuel 135, 492–497. https://doi.org/10.1016/j.fuel.2014.07.005.

Sun, Y., Guo, S., 2018. Characterization of whole-aperture pore structure and its effect on methane adsorption capacity for transitional shales. Energy Fuels 32 (3), 3176–3188. https://doi.org/10.1021/acs.energyfuels.7b03807.

Sun, M., Yu, B., Chen, S., Xia, W., Ye, R., 2015. Reservoir characteristics and adsorption capacity of the lower Cambrian Niutitang Formation shale in southeast of Chongqing: A case study of well Yuke l and well Youke l. Journal of Northeast Petroleum University 39 (1), 69–79.

Sun, M., Yu, B., Hu, Q., Chen, S., Xia, W., Ye, R., 2016. Nanoscale pore characteristics of the Lower Cambrian Niutitang Formation Shale: a case study from Well yuke# 1 in the Southeast of Chongqing, China. Int. J. Coal Geol. 154, 16–29. https://doi.org/10.1016/j.coal.2015.11.015.

Sun, N., Wang, Y., Bai, X., 2017. Thermal fragmentation and pulverization characteristic during pyrolysis of Huadian oil shale. CIE J. 68 (10), 3959–3966. https://doi.org/10.11949/j.issn.0438-1157.20170508.

Sun, L., Tuo, J., Zhang, M., Wu, C., Chai, S., 2019a. Pore structures and fractal characteristics of nano-pores in shale of Lucaogou formation from Junggar Basin during water pressure-controlled artificial pyrolysis. J. Anal. Appl. Pyrolysis 140, 404–412. https://doi.org/10.1016/j.jaap.2019.04.020.

Sun, J., Xiao, X., Cheng, P., Tian, H., 2019b. Formation and evolution of nanopores in shales and its impact on retained oil during oil generation and expulsion based on pyrolysis experiments. J. Petrol. Sci. Eng. 176, 509–520. https://doi.org/10.1016/j.petrol.2019.01.071.

Sun, W., Zuo, Y., Wu, Z., Liu, H., Zheng, L., Wang, H., Sui, Y., Lou, Y., Xi, S., Li, T., Luo, X., 2020a. Pore characteristics and evolution mechanism of shale in a complex tectonic area: case study of the Lower Cambrian Niutitang Formation in Northern Guizhou, Southwest China. J. Petrol. Sci. Eng. 193, 107373. https://doi.org/10.1016/j.petrol.2020.107373.

Sun, W., Zuo, Y., Wang, S., Wu, Z., Liu, H., Zheng, L., Lou, Y., 2020b. Pore structures of shale cores in different tectonic locations in the complex tectonic region: A case study of the Niutitang Formation in Northern Guizhou, Southwest China. J. Nat. Gas Sci. Eng. 80, 103398. https://doi.org/10.1016/j.jngse.2020.103398.

Sun, L., Fu, D., Wu, Y., Wang, Z., 2022. The current study and development of organic matter pores in organic-rich shale. Arabian J. Geosci. 15 (1), 62.

Swami, V., Settari, A., 2012. A pore scale gas flow model for shale gas reservoir. In: SPE Unconventional Resources Conference/Gas Technology Symposium. SPE. https://doi.org/10.2118/155756-MS. SPE-155756.

Tan, J., Hu, R., Luo, W., Ma, Z., He, G., 2021. Pore evolution of lacustrine organic-rich shales: Insights from thermal simulation experiments. Energy Fuels 35 (4), 3079–3094. https://doi.org/10.1021/acs.energyfuels.0c03828.

Tang, X., Jiang, Z., Li, Z., Gao, Z., Bai, Y., Zhao, S., Feng, J., 2015a. The effect of the variation in material composition on the heterogeneous pore structure of high-maturity shale of the Silurian Longmaxi formation in the southeastern Sichuan Basin, China. J. Nat. Gas Sci. Eng. 23, 464–473. https://doi.org/10.1016/j.jngse.2015.02.031.

Tang, X., Zhang, J., Jin, Z., Xiong, J., Lin, L., Yu, Y., Han, S., 2015b. Experimental investigation of thermal maturation on shale reservoir properties from hydrous pyrolysis of Chang 7 shale, Ordos Basin. Mar. Petrol. Geol. 64, 165–172. https://doi.org/10.1016/j.marpetgeo.2015.02.046.

Tang, L., Song, Y., Jiang, Z., Jiang, S., Li, Q., 2019. Pore structure and fractal characteristics of distinct thermally mature shales. Energy Fuels 33 (6), 5116–5128. https://doi.org/10.1021/acs.energyfuels.9b00885.

Tang, Y., Hou, C., He, Y., Wang, Y., Chen, Y., Rui, Z., 2021. Review on pore structure characterization and microscopic flow mechanism of CO2 flooding in porous media. Energy Technol. 9 (1), 2000787. https://doi.org/10.1002/ente.202000787.

Tao, C., Wang, Y., Ni, X., Han, J., Liu, C., 2023. Shale gas geological characteristics and exploration potential of Lower Permian Taiyuan Formation in linxing area. Coal Sci. Technol. 51 (5), 140–148. https://doi.org/10.13199/j.cnki.cst.2021-1073, 2021.

Tenger, B., Lu, L., Yu, L., Zhang, W., Pan, A., Shen, B., Wang, Y., Yang, Y., Gao, Z., 2021. Formation, preservation and connectivity control of organic pores in shale. Petrol. Explor. Dev. 48 (4), 798–812. https://doi.org/10.1016/S1876-3804(21)60067-8.

Thana'Ani, N.A.A., Mustapha, K.A., Idris, M., 2022. Source rock pyrolysis and bulk kinetic modelling of Miocene sedimentary sequences in southeastern Sabah, Malaysia: the variability of thermal maturity to oil-gas producing kerogen. J. Petrol. Sci. Eng. 208, 109513. https://doi.org/10.1016/j.petrol.2021.109513.

Tian, S.C., Wang, T.Y., Li, G.S., Sheng, M., Ren, W.X., 2017. Molecular simulation of methane adsorption behavior in different shale kerogen types. Nat. Gas. Ind. 37 (12), 18–25.

Tissot, B.P., Pelet, R., Ungerer, P.H., 1987. Thermal history of sedimentary basins, maturation indices, and kinetics of oil and gas generation. AAPG (Am. Assoc. Pet. Geol.) Bull. 71 (12), 1445–1466. https://doi.org/10.1306/703C80E7-1707-11D7-8645000102C1865D.

Topór, T., Derkowski, A., Ziemiański, P., Szczurowski, J., McCarty, D.K., 2017. The effect of organic matter maturation and porosity evolution on methane storage potential in the Baltic Basin (Poland) shale-gas reservoir. Int. J. Coal Geol. 180, 46–56. https://doi.org/10.1016/j.coal.2017.07.005.

Tripathy, A., Kumar, A., Srinivasan, V., Singh, K.H., Singh, T.N., 2019. Fractal analysis and spatial disposition of porosity in major indian gas shales using low-pressure nitrogen adsorption and advanced image segmentation. J. Nat. Gas Sci. Eng. 72, 103009. https://doi.org/10.1016/j.jngse.2019.103009.

Ungerer, P., Collell, J., Yiannourakou, M., 2015. Molecular modeling of the volumetric and thermodynamic properties of kerogen: influence of organic type and maturity. Energy Fuels 29 (1), 91–105. https://doi.org/10.1021/ef502154k.

Valentine, B.J., Hackley, P.C., Hatcherian, J.J., 2021. Hydrous pyrolysis of New Albany Shale: a study examining maturation changes and porosity development. Mar. Petrol. Geol. 134, 105368. https://doi.org/10.1016/j.marpetgeo.2021.105368.

Van Krevelen, D.W., 1950. Graphical-statistical method for the study of structure and reaction processes of coal. Fuel 29, 269–284.

Van Krevelen, D.W., 1984. Organic geochemistry-old and new. Org. Geochem. 6, 1–10. https://doi.org/10.1016/0146-6380(84)90021-4.

Veselinovic, D., Dick, M., Muir, C., Green, D., 2018. Measurement of natural gas isotherms and imaging gas in shale using NMR. In: Unconventional Resources Technology Conference. Society of Exploration Geophysicists, American Association of Petroleum Geologists, Society of Petroleum Engineers, Houston, Texas, pp. 2307–2314.. https://doi.org/10.15530/urtec-2018-2886080.

Wang, T., 2000. Immature oils in China and their genetic mechanisms. Acta Geologica Sinica-English Edition 74 (3), 632–640. https://doi.org/10.1111/j.1755-6724.2000.tb00035.x.

Wang, Z., 2019. Reservoir formation conditions and key efficient exploration & development technologies for marine shale gas fields in Fuling area, South China. Acta Pet. Sin. 40 (3), 370. https://doi.org/10.7623/syxb201903011.

Wang, L., Cao, H., 2016. Probable mechanism of organic pores evolution in shale: case study in Dalong Formation, Lower Yangtze area, China. Journal of Natural Gas Geoscience 1 (4), 295–298. https://doi.org/10.1016/j.jnggs.2016.08.005.

Wang, F., Guo, S., 2019. Influential factors and model of shale pore evolution: a case study of a continental shale from the Ordos Basin. Mar. Petrol. Geol. 102, 271–282. https://doi.org/10.1016/j.marpetgeo.2018.12.045.

Wang, F., Guo, S., 2020. Upper paleozoic transitional shale gas enrichment factors: A case study of typical areas in China. Minerals 10 (2), 194. https://doi.org/10.3390/min10020194.

Wang, F., Guan, J., Feng, W., Bao, L., 2013. Evolution of overmature marine shale porosity and implication to the free gas volume. Petrol. Explor. Dev. 40 (6), 819–824. https://doi.org/10.1016/S1876-3804(13)60111-1.

Wang, P., Jiang, Z., Chen, L., Yin, L., Li, Z., Zhang, C., Tang, X., Wang, G., 2016. Pore structure characterization for the Longmaxi and Niutitang shales in the Upper Yangtze Platform, South China: Evidence from focused ion beam–He ion microscopy, nano-computerized tomography and gas adsorption analysis. Mar. Petrol. Geol. 77, 1323–1337. https://doi.org/10.1016/j.marpetgeo.2016.09.001.

Wang, Y., Li, X., Chen, B., Wu, W., Dong, D., Han, J., Ma, J., Dai, B., Wang, H., 2018. Lower limit of thermal maturity for the carbonization of organic matter in marine shale and its exploration risk. Petrol. Explor. Dev. 45 (3), 402–411. https://doi.org/10.1016/S1876-3804(18)30045-4.

Wang, Y., Liu, L., Sheng, Y., Wang, X., Zheng, S., Luo, Z., 2019a. Investigation of supercritical methane adsorption of overmature shale in Wufeng-Longmaxi Formation, southern Sichuan Basin, China. Energy Fuels 33 (3), 2078–2089. https://doi.org/10.1021/acs.energyfuels.8b04344.

Wang, X., Jiang, Z., Jiang, S., Chang, J., Li, X., Wang, X., Zhu, L., 2019b. Pore evolution and formation mechanism of organic-rich shales in the whole process of hydrocarbon generation: study of artificial and natural shale samples. Energy Fuels 34 (1), 332–347. https://doi.org/10.1021/acs.energyfuels.9b03789.

Wang, X., Liu, L., Wang, Y., Sheng, Y., Zheng, S., Wu, W., Luo, Z., 2020a. Comparison of the pore structures of Lower Silurian Longmaxi Formation shales with different lithofacies in the southern Sichuan Basin, China. J. Nat. Gas Sci. Eng. 81, 103419. https://doi.org/10.1016/j.jngse.2020.103419.

Wang, Y., Xu, S., Hao, F., Zhang, B., Shu, Z., Gou, Q., Lu, Y., Cong, F., 2020b. Multiscale petrographic heterogeneity and their implications for the nanoporous system of the Wufeng-Longmaxi shales in Jiaoshiba area, Southeast China: response to depositional-diagenetic process. GSA Bulletin 132 (7–8), 1704–1721. https://doi.org/10.1130/B35324.1.

Wang, P., Zhang, C., Li, X., Zhang, K., Yuan, Y., Zang, X., Cui, W., Liu, S., Jiang, Z., 2020c. Organic matter pores structure and evolution in shales based on the he ion microscopy (HIM): A case study from the Triassic Yanchang, Lower Silurian Longmaxi and Lower Cambrian Niutitang shales in China. J. Nat. Gas Sci. Eng. 84, 103682. https://doi.org/10.1016/j.jngse.2020.103682.

Wang, H., Zhou, S., Zhang, J., Feng, Z., Jiao, P., Zhang, L., Zhang, Q., 2021. Clarifying the effect of clay minerals on methane adsorption capacity of marine shales in Sichuan Basin, China. Energies 14 (20), 6836. https://doi.org/10.3390/en14206836.

Wang, W., Ji, L., Song, D., Zhang, D., Lü, C., Su, L., 2022. Origin of inorganic carbon dioxide associated with hydrocarbon generation: evidence from hydrous pyrolysis experiments and natural and shale gases. J. Asian Earth Sci. X 7, 100079. https://doi.org/10.1016/j.jaesx.2021.100079.

Waples, D.W., 1980. Time and temperature in petroleum formation: application of Lopatin's method to petroleum exploration. AAPG (Am. Assoc. Pet. Geol.) Bull. 64 (6), 916–926. https://doi.org/10.1306/2F9193D2-16CE-11D7-8645000102C1865D.

Wei, M., Zhang, L., Xiong, Y., Peng, P.A., 2019. Main factors influencing the development of nanopores in over-mature, organic-rich shales. Int. J. Coal Geol. 212, 103233. https://doi.org/10.1016/j.coal.2019.103233.

Wei, S., He, S., Pan, Z., Zhai, G., Dong, T., Guo, X., Yang, R., Han, Y., Yang, W., 2020. Characteristics and evolution of pyrobitumen-hosted pores of the overmature Lower Cambrian Shuijingtuo Shale in the south of Huangling anticline, Yichang area, China: Evidence from FE-SEM petrography. Mar. Petrol. Geol. 116, 104303. https://doi.org/10.1016/j.marpetgeo.2020.104303.

Welte, D.H., Tissot, P.B., 1984. Petroleum formation and occurrence. Springer-verlag.
Wenger, L.M., Davis, C.L., Isaksen, G.H., 2002. Multiple controls on petroleum biodegradation and impact on oil quality. SPE Reservoir Eval. Eng. 5 (5), 375–383. https://doi.org/10.2118/80168-PA.
Wu, Y., Fan, T., Jiang, S., Yang, X., Ding, H., Meng, M., Wei, D., 2015a. Methane adsorption capacities of the lower paleozoic marine shales in the Yangtze Platform, South China. Energy Fuels 29 (7), 4160–4167. https://doi.org/10.1021/acs.energyfuels.5b00286.
Wu, S., Zhu, R., Cui, J., et al., 2015b. Characteristics of lacustrine shale porosity evolution, Triassic Chang 7 member, Ordos Basin, NW China. Petrol. Explor. Dev. 42 (2), 185–195. https://doi.org/10.1016/S1876-3804(15)30005-7.
Wu, L., Wang, P., Geng, A., 2019. Later stage gas generation in shale gas systems based on pyrolysis in closed and semi-closed systems. Int. J. Coal Geol. 206, 80–90. https://doi.org/10.1016/j.coal.2019.03.011.
Xi, Z., Tang, S., Zhang, S., Lash, G.G., Ye, Y., 2022. Controls of marine shale gas accumulation in the eastern periphery of the Sichuan Basin, South China. Int. J. Coal Geol. 251, 103939. https://doi.org/10.1016/j.coal.2022.103939.
Xiao, X.M., Wei, Q., Gai, H.F., Li, T.F., Wang, M.L., Pan, L., Chen, J., Tian, H., 2015a. Main controlling factors and enrichment area evaluation of shale gas of the Lower Paleozoic marine strata in South China. Pet. Sci. 12 (4), 573–586. https://doi.org/10.1007/s12182-015-0057-2.
Xiao, X., Wang, M., Wei, Q., Tian, H., Pan, L., Li, T., 2015b. Evaluation of Lower Paleozoic shale with shale gas prospect in South China. Nat. Gas Geosci. 26 (8), 1433–1445. https://doi.org/10.11764/j.issn.1672.
Xie, W., Wang, M., Duan, H., 2021a. Adsorption characteristics and controlling factors of $CH_4$ on coal-measure shale, Hedong Coalfield. Minerals 11 (1), 63. https://doi.org/10.3390/min11010063.
Xie, W., Wang, M., Wang, H., Ma, R., Duan, H., 2021b. Diagenesis of shale and its control on pore structure, a case study from typical marine, transitional and continental shales. Front. Earth Sci. 15 (2), 378–394.
Xie, W., Wang, M., Wang, H., 2021c. Adsorption characteristics of CH4 and CO2 in shale at high pressure and temperature. ACS Omega 6 (28), 18527–18536. https://doi.org/10.1021/acsomega.1c02921.
Xie, W., Chen, S., Vandeginste, V., Yu, Z., Wang, H., Wang, M., 2022a. Review of the effect of diagenetic evolution of shale reservoir on the pore structure and adsorption capacity of clay minerals. Energy Fuels 36 (9), 4728–4745. https://doi.org/10.1021/acs.energyfuels.2c00675.
Xie, W., Gan, H., Chen, C., Vandeginste, V., Chen, S., Wang, M., Wang, J., Yu, Z., 2022b. A model for superimposed coalbed methane, shale gas and tight sandstone reservoirs, Taiyuan Formation, Yushe-Wuxiang Block, eastern Qinshui Basin. Sci. Rep. 12 (1), 11455. https://doi.org/10.1038/s41598-022-15868-2.
Xie, W., Wang, H., Vandeginste, V., Chen, S., Gan, H., Wang, M., Yu, Z., 2023. Thermodynamic and kinetic affinity of $CO_2$ relative to $CH_4$ and their pressure, temperature and pore structure sensitivity in the competitive adsorption system in shale gas reservoirs. Energy 277, 127591. https://doi.org/10.1016/j.energy.2023.127591.
Xing, M., Xu, C., Zhou, G., Sun, L., Du, W., 2021. Experimental investigation for effect of multicomponent inorganic-organic acid solution on pore structure of lignite. Powder Technol. 392, 503–513. https://doi.org/10.1016/j.powtec.2021.07.014.
Xu, Q., Xu, F., Jiang, B., Zhao, Y., Zhao, X., Ding, R., Wang, J., 2018. Geology and transitional shale gas resource potentials in the Ningwu Basin, China. Energy Explor. Exploit. 36 (6), 1482–1497. https://doi.org/10.1177/0144598718772316.
Xu, L., Yang, K., Zhang, L., Liu, L., Jiang, Z., Li, X., 2021a. Organic-induced nanoscale pore structure and adsorption capacity variability during artificial thermal maturation: pyrolysis study of the Mesoproterozoic Xiamaling marine shale from Zhangjiakou, Hebei, China. J. Petrol. Sci. Eng. 202, 108502. https://doi.org/10.1016/j.petrol.2021.108502.
Xu, J., Wu, S., Liu, J., Yuan, Y., Cui, J., Su, L., Jiang, X., Wang, J., 2021b. New insights into controlling factors of pore evolution in organic-rich shale. Energy Fuels 35 (6), 4858–4873. https://doi.org/10.1021/acs.energyfuels.0c04189.
Xu, L., Huang, S., Liu, Z., Wen, Y., Zhou, X., Zhang, Y., Li, X., Wang, D., Luo, F., Chen, C., 2021c. Geological controls of shale gas accumulation and enrichment mechanism in Lower Cambrian Niutitang Formation of western Hubei, Middle Yangtze, China. Front. Earth Sci. 15 (2), 310–331.
Xu, L., Yang, K., Wei, H., Liu, L., Li, X., Chen, L., Xu, T., Wang, X., 2021d. Diagenetic evolution sequence and pore evolution model of Mesoproterozoic Xiamaling organic-rich shale in Zhangjiakou, Hebei, based on pyrolysis simulation experiments. Mar. Petrol. Geol. 132, 105233. https://doi.org/10.1016/j.marpetgeo.2021.105233.
Yang, Y., Bao, F., 2017. Characteristics of shale nanopore system and its internal gas flow: a case study of the lower Silurian Longmaxi Formation shale from Sichuan Basin, China. Journal of Natural Gas Geoscience 2 (5–6), 303–311. https://doi.org/10.1016/j.jnggs.2017.11.001.
Yang, F., Ning, Z., Liu, H., 2014. Fractal characteristics of shales from a shale gas reservoir in the Sichuan Basin, China. Fuel 115, 378–384. https://doi.org/10.1016/j.fuel.2013.07.040.
Yang, F., Ning, Z., Wang, Q., Zhang, R., Krooss, B.M., 2016a. Pore structure characteristics of lower Silurian shales in the southern Sichuan Basin, China: Insights to pore development and gas storage mechanism. Int. J. Coal Geol. 156, 12–24. https://doi.org/10.1016/j.coal.2015.12.015.
Yang, R., He, S., Yi, J., Hu, Q., 2016b. Nano-scale pore structure and fractal dimension of organic-rich Wufeng-Longmaxi shale from Jiaoshiba area, Sichuan Basin: Investigations using FE-SEM, gas adsorption and helium pycnometry. Mar. Petrol. Geol. 70, 27–45. https://doi.org/10.1016/j.marpetgeo.2015.11.019.
Yang, Y., Wang, K., Zhang, L., Sun, H., Zhang, K., Ma, J., 2019. Pore-scale simulation of shale oil flow based on pore network model. Fuel 251, 683–692. https://doi.org/10.1016/j.fuel.2019.03.083.
Yang, W., Yang, R., Wang, M., Bao, S., Yang, L., Hou, H., Song, Y., Jiang, Z., Miao, K., Xu, L., 2025. Impact of lithofacies categories on inflection-point behaviors in micro-nano pore-structure evolution: Implications for differential reservoir-forming mechanisms and “sweet-spot intervals” identification for marine gas shales. Mar. Petrol. Geol. 176, 107336. https://doi.org/10.1016/j.marpetgeo.2025.107336.
Ye, Y.H., Luo, C., Liu, S.G., Xiao, C., Ran, B., Sun, W., Yang, D., Luba, J., Zeng, X., 2017. Characteristics of black shale reservoirs and controlling factors of gas adsorption in the lower Cambrian Niutitang formation in the southern Yangtze Basin margin, China. Energy Fuels 31 (7), 6876–6894. https://doi.org/10.1021/acs.energyfuels.7b00799.
Yi, J., Bao, H., Zheng, A., Zhang, B., Shu, Z., Li, J., Wang, C., 2019. Main factors controlling marine shale gas enrichment and high-yield wells in South China: A case study of the Fuling shale gas field. Mar. Petrol. Geol. 103, 114–125. https://doi.org/10.1016/j.marpetgeo.2019.01.024.
Yin, J., Ju, Y., Lu, S., Li, J., Wang, G., 2017. Nanopores and adsorptivity characteristics of shale. J. Nanosci. Nanotechnol. 17 (9), 6452–6458.
Yu, K., Zhao, K., Ju, Y., 2022. A comparative study of the permeability enhancement in coal and clay-rich shale by hydraulic fracturing using nano-CT and SEM image analysis. Appl. Clay Sci. 218, 106430. https://doi.org/10.1016/j.clay.2022.106430.
Yuan, W., Pan, Z., Li, X., Yang, Y., Zhao, C., Connell, L.D., Li, S., He, J., 2014. Experimental study and modelling of methane adsorption and diffusion in shale. Fuel 117, 509–519. https://doi.org/10.1016/j.fuel.2013.09.046.
Yuan, Y., Rezaee, R., Al-Khdheeawi, E.A., Hu, S.Y., Verrall, M., Zou, J., Liu, K., 2019. Impact of composition on pore structure properties in shale: implications for micro-/mesopore volume and surface area prediction. Energy Fuels 33 (10), 9619–9628. https://doi.org/10.1021/acs.energyfuels.9b02232.
Yuan, Y., Rezaee, R., Yu, H., Zou, J., Liu, K., Zhang, Y., 2021. Compositional controls on nanopore structure in different shale lithofacies: A comparison with pure clays and isolated kerogens. Fuel 303, 121079. https://doi.org/10.1016/j.fuel.2021.121079.
Zhang, M., Fu, X., 2018. Study of the characteristics of marine–terrigenous facies shale from the permo-carboniferous System in the Guxian block, Southwest Qinshui Basin. Energy Fuels 32 (2), 1096–1109. https://doi.org/10.1021/acs.energyfuels.7b02556.
Zhang, S., Su, J., Wang, X., Zhu, G., Yang, H., Liu, K., Li, Z., 2011. Geochemistry of Palaeozoic marine petroleum from the Tarim Basin, NW China: Part 3. Thermal cracking of liquid hydrocarbons and gas washing as the major mechanisms for deep gas condensate accumulations. Org. Geochem. 42 (11), 1394–1410. https://doi.org/10.1016/j.orggeochem.2011.08.013.
Zhang, T., Yang, Y., Gong, Q., Xing, L., Liang, X., Wei, X., 2014. Characteristics and mechanisms of the micro-pores in the early Palaeozoic marine shale, southern Sichuan Basin. Acta Geol. Sin. 88 (9), 1728–1740. https://doi.org/10.19762/j.cnki.dizhixuebao.2014.09.009.
Zhang, X., Shi, W., Xu, Q., Wang, R., Xu, Z., Wang, J., Wang, C., Yuan, Q., 2015a. Reservoir characteristics and controlling factors of shale gas in Jiaoshiba area, Sichuan Basin. Acta Pet. Sin. 36 (8), 926. https://doi.org/10.7623/syxb201508004.
Zhang, J., Liu, K., Clennell, M.B., Dewhurst, D.N., Pervukhina, M., 2015b. Molecular simulation of $CO_2$–$CH_4$ competitive adsorption and induced coal swelling. Fuel 160, 309–317. https://doi.org/10.1016/j.fuel.2015.07.092.
Zhang, L., Li, B., Jiang, S., Xiao, D., Lu, S., Zhang, Y., Gong, C., Chen, L., 2018a. Heterogeneity characterization of the lower Silurian Longmaxi marine shale in the Pengshui area, South China. Int. J. Coal Geol. 195, 250–266. https://doi.org/10.1016/j.coal.2018.05.015.
Zhang, J., Li, X., Zhang, X., Zhang, M., Cong, G., Zhang, G., Wang, F., 2018b. Geochemical and geological characterization of marine–continental transitional shales from Longtan Formation in Yangtze area, South China. Mar. Petrol. Geol. 96, 1–15. https://doi.org/10.1016/j.marpetgeo.2018.05.020.
Zhang, S., Liu, H., Wang, M., Liu, X., Liu, H., Bao, Y., Wang, W., Li, R., Luo, X., Fang, Z., 2019. Shale pore characteristics of Shahejie Formation: implication for pore evolution of shale oil reservoirs in Dongying sag, North China. Petroleum Research 4 (2), 113–124. https://doi.org/10.1016/j.ptlrs.2019.01.002.
Zhang, W., Huang, Z., Li, X., Chen, J., Guo, X., Pan, Y., Liu, B., 2020a. Estimation of organic and inorganic porosity in shale by NMR method, insights from marine shales with different maturities. J. Nat. Gas Sci. Eng. 78, 103290. https://doi.org/10.1016/j.jngse.2020.103290.
Zhang, Y., Yu, B., Pan, Z., Hou, C., Zuo, Q., Sun, M., 2020b. Effect of thermal maturity on shale pore structure: a combined study using extracted organic matter and bulk shale from Sichuan Basin, China. J. Nat. Gas Sci. Eng. 74, 103089. https://doi.org/10.1016/j.jngse.2019.103089.
Zhang, Q., Liu, Z., Liu, C., Zhu, X., Steel, R.J., Tian, H., Wang, K., Song, Z., 2021. Experimental study on the development characteristics and controlling factors of microscopic organic matter pore and fracture system in shale. Front. Earth Sci. 9, 773960. https://doi.org/10.3389/feart.2021.773960.
Zhao, W., Li, J., Yang, T., Wang, S., Huang, J., 2016. Geological difference and its significance of marine shale gases in South China. Petrol. Explor. Dev. 43 (4), 547–559. https://doi.org/10.1016/S1876-3804(16)30065-9.

Zhao, J., Jin, Z., Jin, Z., Hu, Q., Hu, Z., Du, W., Yan, C., Geng, Y., 2017. Mineral types and organic matters of the Ordovician-Silurian Wufeng and Longmaxi Shale in the Sichuan Basin, China: Implications for pore systems, diagenetic pathways, and reservoir quality in fine-grained sedimentary rocks. Mar. Petrol. Geol. 86, 655–674. https://doi.org/10.1016/j.marpetgeo.2017.06.031.

Zhao, T., Li, X., Ning, Z., Zhao, H., Zhang, J., Zhao, W., 2018. Pore structure and adsorption behavior of shale gas reservoir with influence of maturity: A case study of Lower Silurian Longmaxi Formation in China. Arabian J. Geosci. 11 (13), 353.

Zhao, J., Jin, Z., Hu, Q., Liu, K., Liu, G., Gao, B., Liu, Z., Zhang, Y., Wang, R., 2019. Geological controls on the accumulation of shale gas: a case study of the early Cambrian shale in the Upper Yangtze area. Mar. Petrol. Geol. 107, 423–437. https://doi.org/10.1016/j.marpetgeo.2019.05.014.

Zheng, Y., Jiang, C., Liao, Y., 2020. Relationship between hydrocarbon gas generation and kerogen structural evolution revealed by closed system pyrolysis and quantitative Py-GC analysis of a type II kerogen. Energy Fuels 35 (1), 251–263. https://doi.org/10.1021/acs.energyfuels.0c02468.

Zhong, J., Chen, G., Lv, C., Yang, W., Xu, Y., Yang, S., Xue, L., 2016. Experimental study of the impact on methane adsorption capacity of continental shales with thermal evolution. Journal of Natural Gas Geoscience 1 (2), 165–172. https://doi.org/10.1016/j.jnggs.2015.12.001.

Zhou, S., Wang, H., Xue, H., Guo, W., Lu, B., 2016. Difference between excess and absolute adsorption capacity of shale and a new shale gas reserve calculation method. Nat. Gas. Ind. 36 (11), 12–20.

Zhou, J., Liu, S., Zhou, N., et al., 2018. Development and application of a continuous fast microwave pyrolysis system for sewage sludge utilization. Bioresour. Technol. 256, 295–301. https://doi.org/10.1016/j.biortech.2018.02.034.

Zhou, N., Lu, S., Zhang, P., Wang, M., Xiao, D., Li, J., Chen, G., Zhang, Y., Wang, J., Lin, Z., 2022. Continental shale gas dynamic enrichment and evolution over geological time. Int. J. Coal Geol. 251, 103914. https://doi.org/10.1016/j.coal.2021.103914.

Zhu, Z., Yao, G., Lou, Z., Jin, A., Zhu, R., Jin, C., Chen, C., 2018a. Upper Paleozoic marine shale characteristics and exploration prospects in the Northwestern Guizhong depression, South China. J. Ocean Univ. China 17 (4), 773–790.

Zhu, H., Ju, Y., Qi, Y., Huang, C., Zhang, L., 2018b. Impact of tectonism on pore type and pore structure evolution in organic-rich shale: implications for gas storage and migration pathways in naturally deformed rocks. Fuel 228, 272–289. https://doi.org/10.1016/j.fuel.2018.04.137.

Zhu, Y., Li, Z., Zeng, L., Liu, Z., Wang, X., 2022. Diagenesis and its impact on the reservoir quality of continental shales: a case study of the Lower Jurassic Da'anzhai Member of the Ziliujing Formation in the Sichuan Basin, China. Geofluids 2022 (1), 5942370. https://doi.org/10.1155/2022/5942370.

Zou, C., Zhao, Q., Cong, L., Wang, H., Shi, Z., Wu, J., Pan, S., 2021. Development progress, potential and prospect of shale gas in China. Nat. Gas. Ind. 41 (1), 1–14.